Pressure and Basin Modeling in Foothill Belts

Jean-Paul Callot, Kevin Hill, Renaud Divies, Nigel Wilson, William Sassi, François Roure

Pressure and Basin modelling in foothills belts: A Ceres study of the Kutubu area, Papua New Guinea fold and thrust belt.

Jean-Paul Callot[1, $,*], Kevin Hill[2], Renaud Divies[3], Nigel Wilson[2], William Sassi[1], François Roure[1]

[1]*IFP Energies Nouvelles, 1 et 4 Av. de Bois-Préau, 92852 Rueil-Malmaison cedex, France.*

[2]*Oil Search limited, 22 Floor, 1 Bligh Street, Sydney, NSW Australia 2000.*

[3]*Beicip Franlab, 282 av. Napoléon Bonaparte, 92852, Rueil Malmaison cedex, France.*

$ Now at LFCR, Université de Pau et de Pays de l'Adour, Avenue de l'Université, 64013 Pau, France

** Corresponding author; jean-paul.callot@univ-pau.fr*

Abstract

The Papua New Guinea fold and thrust belt petroleum system is studied along a 200km long transect. The kinematic scenario includes the Jurassic rifting and passive margin, the erosion during the Upper Cretaceous related to the Coral Sea rifting and Plio-Pleistocene shortening, with an early growth of the Hedinia anticline limiting lateral migration of oil, in the adjacent Darai Plateau. Data from seven wells and two fields were used to calibrate section boundary conditions and properties. Apart from the high pressure trend in the Kutubu/Moran structures, all data are well reproduced, and the modelled section appears quantitatively predictive. The modelling demonstrates three major pathways for water: (1) topographically driven flow, from the onset of mountain building, (2) deep updip basinal flux, flowing along the tilted reservoirs, and (3) across fault escape from connected reservoir bodies. Type II or mixed type II/III are used to model the Triassic and Jurassic source rock. Maturation starts in the mid Cretaceous and increases strongly during the late tectonic burial, with three main accumulations: (1) the deep part of the Mubi zone, with vertical migration along faults; (2) the Hedinia and Kutubu anticlines charged during Orubadi and Era deposition; and (3) the Darai plateau.

Keywords: Papua New Guinea, Fold and Thrust Belt, Basin Modelling, Pressure, Petroleum system

1. Introduction

Globally, most of the easy-to-find oil and gas prospects have been drilled and the industry is exploring in increasingly difficult terrains such as in tectonically complex mountain belts or in deep water. Discoveries are often at great depth and structural complexity and require

sophisticated geological and geophysical modelling. The recent improvements in seismic imaging (e.g. Naville et al., 2010) have led to the discovery of giant petroleum fields in deep underthrust prospects of the Sub-Andean basins in Venezuela (El Furrial discovery) and Colombia (Cusiana discovery, Carnevalli, 1988; Cooper, 1995; 2007), and similar efforts are being made in the Papua New Guinea fold and thrust belt (hereafter termed the Papuan Fold Belt; Hill et al., 2008). However, these structurally complex areas retain a high risk and it is imperative to understand the whole petroleum system to mitigate that risk. In particular, charge risk can be assessed from estimates of paleothermal gradients, paleofluid flow and pore pressure, and the relative timing between the structural evolution and the petroleum system maturity.

Estimates of paleo-burial and -temperatures in foothills belts are difficult due to the dominant processes of uplift and erosion. In foreland settings or extensional basins where there is limited erosion, the use of well data such as BHT, and paleo-thermometers such as vitrinite reflectance (Ro) and Rock-Eval (Tmax) data are usually sufficient to invert the heat flow and geothermal gradients along a section. However, in the foothills domains erosion affects paleo-burial estimates and the corresponding calibration of the past thermal evolution of the section is biased (e.g. Deville and Sassi, 2006). In particular, it is generally not possible to obtain a single solution for paleo-burial and paleo-thermal gradients if based solely on maturity ranks of the organic matter (e.g. Osadetz et al., 2004; Hardebol et al., 2009; Roure et al., 2009; 2010). An integrated thermo-kinematic approach is required, which allows for predictive modelling of the temperature as a combined effect of sedimentary and tectonic loading, heat advection and erosional process (e.g. Forster and Smith, 1989; Bodri and Rybach, 1998; Husson and Moretti, 2002; Deville and Sassi, 2006; Hardebol et al., 2009).

Pore fluid pressure and overpressure building are an additional challenge in fold and thrust belt exploration. Dewatering of sediments during the compaction phase and associated overpressures has been widely documented in modern accretionary wedges (e.g. the Nankai prism, Tobin and Saffer, 2009). The increasing load of syn-flexural sediments deposited in foredeep basins results in a vertical escape of formation water during mechanical compaction with mainly dominantly hydrostatic pore fluid pressures. However, this process develops a regional pressure seal localized where the vertical permeability reaches a minimum, killing the vertical connectivity and any further escape of compaction-related fluids towards the surface. This process accounts also for the building of an over-pressured horizon in the foreland, which strongly decreases the friction locally, and helps to localize and propagate

forelandward the decollement and the deformation front (e.g. Henry and Wang, 1991; Saffer and Bkins, 1998; Skarbek and Saffer, 2009).

From a simple geometric and structural point of view, fold and thrust belts have many points in common with underwater accretionary wedges, but they differ strongly when considering the fluid pathways, the boundary conditions (pressure and temperature) and the nature of the pre-orogenic and syn-orogenic sequences. In contrast to accretionary wedges, which integrate mostly young and poorly compacted syn-flexural sequences, fold and thrust belts involve dominantly pre-orogenic passive margin sequences, already buried, compacted and dewatered. The origin of the fluids involved during the deformation processes also differs in that fold and thrust belts mix sedimentary fluids with meteoric water and older deeper basinal fluids whereas accretionary wedges are usually entirely marine fluids in offshore accretionary prims. Thus, aerial fold and thrust belts are generally under-saturated in fluids in contrast to completely saturated submarine belts. Thus the driving pressure gradients will not be similarly distributed, and the topographically driven flows may play a first order role. It is particularly true considering the "squeegee" fluid flow associated with the inception of belt building, and with major changes in foreland reservoir properties and oil migration (Oliver, 1986; Machel and Cavell, 1999; Roure et al., 2005; 2010)

Fold and thrust belts are thus characterized (1) by fluid flow controlled by lateral permeability barriers, and (2) by topography-driven, gravitational flow of surface water, following the topographical gradients towards the valleys and the foreland basin (Schneider et al., 2002; Callot et al., 2010; Gonzalez-Mercado et al., 2013). This gravitational flow remains, however, mostly confined above the compaction-induced permeability barrier (see above). Due to the difficulties in acquisition, processing and interpretation of onshore seismic data, the architecture of the subsurface reservoir is usually poorly imaged and its internal compartmentalization is poorly defined. The analysis of fluid dynamics in such a setting requires integrated basin modelling techniques, as documented below, to predict the distribution of pore fluid pressures and hydrocarbon (HC) potential before drilling. Another key factor in sub-thrust plays is reservoir damage due to diagenesis, the understanding of which requires integrating the geometrical evolution of the play, the diagenetic history and the strain history in the framework of the larger scale geometrical evolution, comprising input data from the burial, thermal and pore fluid pressure evolution (e.g. Vilasi et al., 2009; Roure et al., 2009; Gonzalez-Mercado et al., 2013).

Thus, qualitative and quantitative appraisal of the petroleum system evolution and HC potential of given plays in foothills belts requires the integration of various data differing both

in time and space. Basin modelling tools are now better able to reconstruct palinspastic structural cross sections (e.g. Schneider et al., 2003; Roure et al, 2005; 2010; Vilasi et al., 2009; Callot et al., 2010) and compute the history of temperature, pore fluid pressure and fluid flow circulations in complex structural settings. They constitute an efficient tool to integrate, within the framework of the basin geometrical evolution, the various key phenomena controlling the evolution of reservoir properties (e.g. Roure et al., 2005; Vilasi et al., 2009).

Hill et al. (2010) presented a 110 km regional balanced and restored cross-section over the Papuan Fold Belt from the foreland to the hinterland deformed internal belts and passing near the giant Kutubu oil and gas field. Utilising that section, the aim of this paper is to present an integrated study of fluid flow and fluid pathway analysis in the Papuan Fold Belt. The structure of the Papuan Fold Belt is well documented and it formed during the Late Miocene and Pliocene so the timing is well constrained. This allows us to test the ability of the basin modelling tools to predict, in the framework of the fold belt evolution, both the porosity, the pore fluid pressure, and the temperature field evolution through time. The steps involved include kinematic restoration and testing of the section, prediction of temperatures, porosities and pressures through time, constrained by borehole and surface data. This allows hydrocarbon generation and fluid flow to be modelled and tested against known oil and gas fields and well data. This constitutes the first step toward a more predictive description of the potential fluid rock interaction at the fold-belt scale through time, and toward a quantitative assessment of the petroleum potential (e.g. Hill et al., 2010).

2. Geological setting

2.1 Tectonostratigraphic setting

New Guinea forms the northern margin of the Australian plate, within the convergent plate boundaries between the Indo-Australian Plate, the Pacific Plate, and several smaller plates (Figure 1). Following the Triassic New England orogeny, New Guinea underwent extension in the Jurassic, subsidence during the Cretaceous, uplift in the Paleogene and subsidence followed by a compressional orogeny in the Neogene to Recent. The tectonic evolution of New Guinea was reviewed by Hill and Hall (2003), and the reader is referred to that paper and references therein for further details. Here, we only review the events and kinematic evolution relevant to the pressure and basin modelling.

The island of New Guinea has been divided into four tectonic regions based on the Miocene to Holocene orogenesis affecting the northern part of the Australian Plate (Dow, 1977; Hill et al., 1996; Hill et al. 2003). In the south is the Stable Platform, which is the northern continuation of Australian continental crust that preserves Mesozoic and possibly Palaeozoic extensional structures (Cole et al., 2000; Kendrick 2000). To the north, the adjacent Fold Belt comprises the same crust deformed into fold and thrust structures following Late Oligocene–Miocene arc–continent collision. Most of the northern half of New Guinea is made up of the Mobile Belt, including ophiolites of Mesozoic to Palaeocene age (Davies and Jaques, 1984; Rogerson et al., 1987). The Mobile Belt also includes distal Mesozoic–Tertiary sediments, abundant Miocene and some Cretaceous volcanic and intrusive igneous rocks, and medium- to high-grade metamorphic rocks with common Early Miocene and some Mesozoic cooling ages. The northern margin of New Guinea comprises accreted volcanic arcs.

The Tasman Line in Australia (Scheibner 1974) separates Proterozoic basement to the west from accreted Palaeozoic terranes to the east and can be correlated into New Guinea from surface geology and tomographic modelling. In New Guinea, the Tasman Line is roughly north-south along the PNG-Indonesia border, such that basement in PNG largely comprises accreted terranes (Figures 1 and 2). Those dated are of Permian to Early Triassic age and intruded by Middle Triassic granites (Van Wyck and Williams 2002; Crowhurst et al. 2004). The active post-Triassic tectonic history of PNG and the tomographic studies both suggest a young hot and weak lithosphere and geological analyses suggest a strong northeasterly structural grain (Davies 1991; Corbett 1994; Hill et al. 1996).

In the Late Triassic to Jurassic (figure 2A), post-orogenic collapse and rifting occurred in what is now the fold belt and probably led to the breakaway of microcontinental slivers from the northern New Guinea margin. From the late Jurassic through the Cretaceous, the margin underwent passive subsidence with clastic sediment supply from the Australian continent to the south (figure 2B). This steady state was interrupted by uplift of southern and eastern PNG in the Palaeogene, thought to be a thermal response to opening of the Coral Sea to the east (figure 2C). As Australia commenced rapid movement to the north in the Eocene, ophiolites were emplaced along the northern New Guinea margin and carbonates were deposited in the adjacent basins.

The initial collision with an island arc was probably in the late Oligocene (figure 2D), but the Early Miocene was a time of strike slip and extensional tectonics in northern New Guinea, including the unroofing of metamorphic core complexes (Figure 2E). These events coincided with the rapid subsidence of the entire New Guinea margin and the widespread deposition of thick carbonate sequences in the south and volcanics in the north. The onset of regional compression and uplift occurred in the Middle Miocene (figure 2F) and migrated south into what is now the fold belt in the Late Miocene to Pliocene (Hill, 1991; Hill and Raza 1999; figures 2G-H). In the western part of the Papuan Fold Belt a foreland basin formed and filled and is preserved to the south of the current mountains. In the eastern fold belt, the area of study, a Pliocene-Pleistocene foreland basin is inferred from vitrinite reflectance and fission track data, but the sediments were mostly eroded off during formation of the fold belt.

2.2 Papuan Fold Belt stratigraphy

The basement underlying the Fly Platform and the fold belt comprises Upper Palaeozoic rocks, mainly Permian phyllites, which were deformed during the Triassic New England Orogeny and intruded by granites (Van Wyck and Williams 2002; Crowhurst et al. 2004). Subsequent erosion exposed the granites at that time. Late Triassic to Middle Jurassic rifting created graben in which the Kana Volcanics, Magobu Coal Measures and Barikewa Mudstone were deposited, the latter two being probable source rocks (Figures 3 and 4). Regional Late Jurassic subsidence flooded the margin allowing deposition of the Imburu Formation, Toro, Digimu, Iagifu and Hedinia sandstone reservoirs and the Cretaceous Ieru Formation seal. In distal facies of the northeastern Fold Belt, both the Imburu and Ieru mudstones are hydrocarbon source rocks. Latest Cretaceous to Palaeocene uplift of southern PNG caused erosion of some Upper Cretaceous sediments in the fold belt and Fly Platform area and deposition did not resume until Late Oligocene flooding allowed widespread deposition of Miocene shallow marine carbonates, the Darai Limestone. Carbonate deposition was halted by the Late Miocene onset of compressional deformation, which was also responsible for generation and migration of most hydrocarbons.

2.3 Papuan Fold Belt structure

The southern portion of PNG comprises the Fly Platform, which is relatively undeformed by Cenozoic compression. APC (1961) divided the Papuan Fold belt into three northwest-southeast trending belts, the Gently Folded Belt in the south, the Strongly Folded Belt in the centre and the Imbricate Belt to the north (Figures 3 and 4). Hill et al (2010) discussed the

structural styles of these belts and presented a regional balanced and restored cross-section across all of them, which was the input for the current modelling (Figure 4). The section was constructed in 2D Move (®) and was incrementally restored to help validate the interpretation and show the likely forward kinematic evolution. It was (1) drawn to honour all stratigraphy and dips from outcrop and 10 boreholes in addition to synthetic aperture radar images and limited potential field data; and (2) constructed along or close to seismic lines, particularly the semi-regional line PN05-404 (shown in Hill *et al.* 2008) across the Fold Belt.

Fly Platform and Gently Folded Belt

On Figure 4, it can be seen that the thickness of sediments beneath the Darai Plateau is more than double that of the adjacent Fly Platform (4,800m vs 2,200m) indicating a major basin-bounding extensional fault that subsequently underwent mild inversion. Sediment growth across the fault appears to have been continuous through geological time, indicating a relatively stable platform to the south. Compressional offset of the Darai Limestone and continuing earthquake activity suggest that inversion was Pleistocene to Recent, but a component of Late Miocene inversion cannot be ruled out.

The significance of the unconformity between the Cenomanian upper Ieru Formation and the Late Oligocene basal Darai Limestone has been assessed by apatite fission track analyses (*eg*. Hill & Gleadow 1989; 1990) combined with vitrinite reflectance profiles in the Kanau-1 well. These analyses indicate that, prior to Darai Limestone deposition, there was at least 2 km of erosion of the upper Ieru Formation beneath the Darai Plateau, but less than 1 km of erosion beneath the foreland. Thus it is likely that the old normal fault beneath the Darai Plateau was inverted in the Early Tertiary, and that the hanging-wall was eroded prior to regional Oligo-Miocene subsidence.

Strongly Folded Belt

Seismic data and regional gravity data suggest that basement dips at ~6 degree to the NE beneath much of the strongly fold belt with relatively little offset. Although inversion of extensional faults is suspected, for instance the Zongwe structure (Hill et al 2010), it is minor. Thus the large folded structures within this belt, such as Zongwe, Ai-Io and SE Hedinia, are interpreted to be detached within the sedimentary section (Fig. 3). The SE Hedinia anticline has been drilled by three wells, which indicate a tight anticline with an overturned or sheared out forelimb, all detached near the top of the Koi-Iange section. Between SE Hedinia and East

Kutubu (Figure 4) basement faulting is interpreted to have deformed the top Koi-Iange Formation detachment so that at least some basement faulting occurred after the overlying thin-skinned deformation (Hill et al 2010).

Imbricate Belt

Over a distance of 10 km to the NE of the Kutubu East Anticline, interpretation of the seismic data (Hill *et al.* 2008, 2010) indicates a planar gently NE-dipping panel of strata from basement to top Darai Limestone (Figure 4). Geological maps show that this panel is overlain by thrust repeats of Darai Limestone and thin upper Ieru Formation, the start of a major Darai duplex that crops out over a band that is 24 km wide from Lake Kutubu to the Wage Anticline. Beneath the mapped Mubi Anticline the step-up in basement, inferred from seismic data, clearly folds the overlying Darai Limestone duplex, so the basement thrusting occurred after the thin-skinned deformation. The Darai Limestone duplex exposed at surface represents considerable shortening in the Darai Limestone and upper Ieru Formation. Below, or to the NE this must be balanced by equivalent shortening in the lower Ieru Formation to Koi-Iange Formation. On the cross-section, this has been represented as a simple duplex forming the Mount Castle and Wage Anticlines. However, numerous other interpretations are possible, including basement involvement.

2.4 Papuan Fold Belt hydrocarbons

Exploration for hydrocarbons in the Papuan Fold Belt commenced in the 1950's on the accessible mountains, resulting in significant gas discoveries such as Barikewa in 1958 and Juha in 1983. Commercial oil was discovered in 1987 in the Iagifu-Hedinia anticlines (termed the Kutubu oilfield, eg. Bradey et al. 2008) followed by nearby discoveries at Agogo, SE Mananda, Moran and Gobe, which have, collectively, been on production since 1992. Recoverable reserves in the known fields are well over 500 million barrels of low viscosity oil. Along strike, the giant Hides gas field (Johnstone & Emmet, 2000), with over 5 trillion cubic feet (tcf) reserves, was discovered in 1986 and has recently been developed for LNG production. Please note that there is some confusion over the term 'Kutubu'. Lake Kutubu lies just northeast of the Iagifu-Hedinia Anticlines, the main oil producing area in PNG, which is now called the Kutubu Oilfield (Figure 4). Immediately south of the Lake is the separate anticline that makes up Kutubu Mountain, here termed the East Kutubu Anticline. This structure has been drilled by Kutubu-1 and Kutubu-2 wells without success. These wells are analysed as part of this study.

Three oil and gas fields lie near the regional cross-section that is analysed here and nine wells are along or very close to the section. The thermal properties from key wells, such as present temperature and VR data, pore fluid pressure and water table location, have been used to calibrate the modelling and the nearby oil and gas fields have been used to validate models of hydrocarbon generation and migration. In the foreland, the Bujon-1 well drilled a subtle and local basement high and did not encounter significant hydrocarbons. On the giant Darai Plateau (Figs 1 and 3) neither the Kanau-1 nor the Bosavi-1 wells recovered hydrocarbons thought to be due to lack of charge. It is notable that the Toro sandstone reservoir in both wells is near sea level (Fig 4) and that to the SW it almost abuts the basal Darai Limestone across the Darai Fault. It is considered likely that along strike the Toro connects to the basal Darai Limestone and hence is in pressure communication with the foreland, consistent with the low pressures recorded in the Kanau-1 well.

The SE Hedinia-1, -2 and -3 wells drilled the SE Hedinia gas field, whilst along strike the Kutubu oil and gas field (drilled by the Iagifu and Hedinia wells) has produced over 350 million barrels of oil and contains ~1 tcf of gas. Thus on a regional basis, any modelling needs to account for significant oil and gas charge. The East Kutubu anticline (Figs 1 and 3) was drilled by the Kutubu-1 and -2 wells, which encountered minor gas and high pressures at reservoir level, but fractures and oil staining above the reservoir indicate breaching. The Strongly Folded Belt to the southwest preserves normal to low pressures, suggesting a sealing fault underlying the East Kutubu anticline separating the high-pressure belt to the northeast from the adjacent SE Hedinia gasfield and Kutubu oilfield to the southwest. The Nembi well at the NE end of the section (Fig 4) drilled through distal Tertiary limestones and shales and was not analysed here.

2.5 Hydrodynamics in the Papuan Fold Belt

Little has been published about fluid flow in the Papuan Fold Belt. Eisenberg (1993) discussed a hydrodynamic gradient across the Iagifu/Hedinia area (Kutubu oilfield) and noted that, although the reservoir sandstones are all marine, the recovered formation water is quite fresh, typically in the range of 6000-15000 ppm NaCl equivalent. On a regional basis, from maps of hydraulic potential, he inferred that water flows from both SE and NW along the Papuan Fold Belt to the Usano-SE Hedinia area (Fig. 1) where it exits the fold belt to the SW

towards the low pressure foreland. This inferred exit point is very close to the line of cross section studied here.

3. Data set and modelling principles

3.1 Basin modelling in structurally complex areas

Basin modelling aims at reconstructing the time evolution of a sedimentary basin in order to make quantitative predictions of geological phenomena leading to pressure generation and ultimately, to hydrocarbon accumulations. It accounts for porous medium deformation, heat transfer, hydrocarbon formation and multiphasic fluid migration (e.g. Schneider et al., 2000).

Since the pioneer works on the modelling of hydrocarbon formation (Tissot, 1969), several generations of basin models have been built. Initially, 1D models such as Genex were used to simulate the temperature evolution and the maturation of the organic matter. In a sedimentary basin context, the 1D approach is satisfactory for these purposes because the thermal transfers are mostly vertical. Indeed, thermal convective transfers are most frequently negligible. Subsequently, 2D models such as Temispack (Chenet et al., 1986; Bessis et al., 1987; Doligez, 1987; Bessis et al., 1990; Ungerer, 1990; Ungerer et al., 1990) were built. These 2D models made it possible to evaluate the pressure history and to predict hydrocarbon migration and reservoir charge. However, these evaluations are only qualitative because fluid (water, oil, and gas) migration is mainly convective and therefore sensitive to 3D geometry and anisotropy. For these reasons, a generation of 3D basin models, such as Temis 3D or PetroMod was designed (e.g. Schneider et al., 2000).

The previous sedimentary basin models however are only able to handle relatively simple geometries resulting from deposition, erosion and vertical compaction. As exploration is now focusing on complex areas, such as fold belts, a new generation of models able to handle faults is needed (figure 5). The CERES 2D software used in the current study is composed of several modules managed by a study browser. The main modules are a section editor, a restoration module and a forward simulation simulator. The other modules are a chronostratigraphy editor, a lithology editor, a kerogen editor, fluid editors, a mesh editor, a run editor, and visualization modules. The main steps to carry out a case study (figure 5A) are: (1) production of the initial section (figure 5B), (2) restoration of the section (figure 5C) and (3) forward simulation of the section.

3.2 Ceres 2D

3.2.1 Initial section

The initial section is composed of a 2D cross section, which can be edited directly from scratch or can be imported from other software. It is recommended, at this stage to use structural tools to balance the section. The present day geometry of the section is defined first. The geological attributes are then assigned, including labelling of horizons and faults, definition of decollement levels, and finally the distribution of lithology, which may evolve spatially but not in time.

At this stage the blocks, which represent the smallest kinematic units, are defined and meshed with their own grids, with no constraint coming from the other blocks. The fault grids are created dynamically during the forward simulation. The initial section includes the upper mantle, the ductile lower crust, the brittle upper crust and the sedimentary basin.

3.2.2 Kinematic scenario

Once production and editing of the initial section is complete, the evolutionary stages of the sections are created working backward from the present, including kinematic restoration, backstripping, and thickness modification.

For each restoration scenario, the backward process is composed of different steps (Schneider et al., 2002). The first step is restoration of the eroded parts if erosion has occurred during the considered period. Importing templates from other software such as Thrustpack or 2DMove, which can handle forward kinematic modelling, may help the production of intermediate stages. The second step is an automatic backstripping of the section. Once the erosion and the sedimentation have been accounted for, the resulting section is uncompacted using porosity depth relationships. The section is then restored from a kinematic point of view. At this stage, the displacements along faults are accounted for, using translations, vertical shear, and/or flexural slip mechanisms.

The last step of the backward simulation requires the correction of local inconsistencies in the computed thicknesses which result from the use of the vertical shear mode of deformation. This step allows accounting for salt or mud tectonics. Correction of the restored eroded section may be done at this stage. These steps must be performed for each layer as initially defined in the present day section.

3.2.3 Forward simulations

In these complex geometries, faults cut the basin into blocks that naturally define computational subdomains, using Domain Decomposition Methods (DDM, e.g. Faille et al., 1998). In each block, the model accounts for compaction of the porous medium, erosion, heat transfer, and the formation and migration of hydrocarbons (Schneider et al., 2002, 2004; Schneider, 2003). The equations incorporate mass conservation of solid and fluids (water, oil, and gas) coupled with Darcy's law and a compaction law. The faults have a constant thickness and their permeability may evolve with time. The prototype allows using three permeability models for the faults. Faults can be 1) pervious 2) impervious, being a flow barrier, or 3) their permeability can evolve through time according to the properties of neighbouring lithologies. Permeability can also change with the strain rate. Whichever option is chosen, the faults are considered as inactive when their velocities are lower than the defined speed limit of 50m/Ma.

3.2.4 Drawbacks

Although Ceres-2D is a powerful tool, thesoftware still faces numerical limitations that the user must take into account in order to perform reliable modelling and analysis of results. Two main drawbacks need to be discussed:

(1) The restoration mode: due to the numerical requirements for fast solution solvers of fluid flow equations, the mesh is based on a set of gridded horizons, representing the real geological events. The grid cells are laterally limited by borders, which remain vertical throughout the simulation. This precludes any displacement between layers, i.e. the flexural slip or flexural flow mode, which is the main deformation mode of a layered sedimentary section in a compressive setting. Thus the modules, which are defined as layered units separated by faults, topographic surfaces, model edges or section base, are only restored through vertical shear. At a given restoration step, only the pre-restoration length and vertical thicknesses are kept constant, although the real lengths and bed-perpendicular thicknesses should be preserved. Therefore, at each restoration step, thickness modifications must be applied to retrieve reliable lengths and thicknesses for each restored model. This is partly automated by a geometric algorithm preserving the bed lengths and correcting the thicknesses in order to preserve the bed surfaces. Such automated procedure limits the amount of manual correction required, but this step remains compulsory.

(2) The topology: It is also compulsory to preserve the ordering of the blocks within the section, each block being a unit separated from the others by faults, model boundaries, and topography/bathymetry. Thus out-of-sequence thrusting is forbidden, as it would change the topological ordering by placing deep blocks on top of blocks that formerly overlay them. One

artificial solution that allows an emerging out-of-sequence thrust to be rooted at depth is to draw fictitious triangle zones.

(3) The faults: faults are fundamental objects for fluid flow pathways in basin modelling (Yielding et al., 1999; Billi et al., 2003). Fault behaviour may range from completely pervious (e.g. active fault or fault having a drain activity, without a cemented or brecciated core) to completely impervious and hence acting as a barrier (e.g. cemented inactive fault or fault sealed by clay smearing) (e.g. Brown 2003; Bretan et al., 2003). The geographic zone surrounding the fault plays itself a role, because the damaged zone can be either a barrier (grain size reduction in numerous shear bands, which constitute cemented zones) dividing the reservoir into compartments, or a drain at a large scale (coalescence of open faults at various scales). The behaviour of the faults can be tuned in different ways in Ceres: either pervious, impervious, or with controlled anisotropic permeabilities. The fault element permeability in the latest case is calculated from the closest rock element permeabilites through a harmonic mean for the transversal permeability and an arithmetic mean for the longitudinal permeability. Taking into account the fault slip rate can modify this anisotropic behaviour. Above a given threshold value, the fault activity will enhance its permeability. In addition, fault rocks can integrate the capillary pressure mechanisms in the computation of the coupled water and hydrocarbon flow.

3.3 Dataset and constraints

Calibration of the basin model was performed against data coming from the nearest wells, projected on the section plane. Nine wells were used (Figures 4 and 6): the Bosavi well in the Fly Platform, the Bujon and Kanau wells from the Darai Plateau, the Iorogabaiu well drilled in the Zongwe trend, the Hedinia 1X and 3X wells drilled in the Hedinia major structures, the Iagifu and Usano wells in the tectonic slices separating Hedinia from Kutubu, and finally the Kutubu wells, which are located near the top of the major Kutubu anticline. Field data from the Mubi tectonic units in the imbricate zone have also been integrated. At each well, reservoirs tops were used to define burial through time. The water table level was used to determine the reference level for the hydrostatic curves. Both values have been used to propose static corrections of the predicted pressure regime. Present day temperature of the reservoirs and maturity data (mostly vitrinite) have been used to constrain the heat flow scenario.

The heat flow evolution with time is a major thermal boundary condition. It is numerically applied at the base of the crust, but incorporates the effect of the radioactive heat production

within the crustal rocks. As this effect is difficult to assess from field, well or potential data, it is included within the total basal heat flow applied at the base of the sedimentary section. The crustal part below the sedimentary basin is therefore transparent to heat. Note that the model takes into account the effect of a possible heat production within the sedimentary section (even if based here on a default value in the absence of control data, such as the amount of radioactive elements for a given lithology).

We consider here a thermal scenario that integrates a first pulse of heat flow related to the Triassic to early Jurassic rifting. The maximum value of heat flow applied here is 80 mW.m-2. The heat flow then decays to a value of 37 mW.m-2 in the mid Cretaceous, followed by a second heat pulse associated to the Coral Sea rifting, reaching a maximum value of 53 mW.m-2. This pulse is associated with uplift of the Papuan margin and erosion of the Ieru Shale. Then the heat flow again decreases close to the present day value of 35 mW.m-2. This scenario is in accordance with the scenarios proposed by AFTA analysis (Cawley and Taylor, 1991, TFN463; Duddy et al., 1991; Geotrack report 282; Green, 2001, Geotrack report 801).

A second boundary condition relates to the surface temperature and the atmospheric gradient. The latter is chosen at 5°C.km-1 and is not considered as a variable for the fit. In contrast, the surface temperature records a progressive increase during the Mid to Late Tertiary, from initial values of ~5°C at sea level during the Palaeozoic and Mesozoic, toward a present value of 30°C at sea level. This boundary condition will have only a minor affect on the deep evolution of the temperature field, but will affect the present day distribution of temperature at shallow depths (up to 1000m).

3.4 Kinematic scenario

The structural evolution of the section is based on a previously studied regional cross section running from the Fly Plateform to the Mubi-Wage hinterland, and crossing the Hedinia and Kutubu trends (Hill et al., 2010). The section has been balanced, although the deep structures in the hinterland, below the imbricate belt, remain speculative.

Several simplifications from the interpreted present day section (Figure 6) have been made. In particular and at a large scale, it is not possible to account for out-of-sequence thrusting, which will locally change the topological ordering of blocks. For instance we have deleted the connection between thrust faults in the cover and their lateral extent within the basement blocks. These faults were activated later in the structural evolution, cutting across the initial decollement level along the deep contact between the Koi-Iange layers and the underlying synrift series. However we kept the spatial and temporal association between the late

inversion of the extensional blocks at depth and the activation/reactivation of thrusted slices in the sedimentary cover. For the purpose of simplification, the Zongwe tectonic slices have been represented as a single thrust unit. In addition, we kept only four tectonic units in the Mubi/Wage area. At depth, we proposed a shallow ramp to account for the vertical uplift associated with these units, with a deep decollement accommodating only a limited amount of shortening.

The kinematic scenario reproduces the following steps in the section evolution (Figure 7):

- Late Triassic rifting and development of tilted blocks, inception of the passive margin stage;
- Infill of the platform/slope/basinal parts during the Jurassic to Cretaceous evolution, with a marked thickening of the Koi-Iange and Iagifu sequences toward the north-east;
- Upper Cretaceous deposition and then erosion of the Ieru Shale, associated with the Coral Sea rifting and regional intraplate uplift;
- Deposition of the Darai carbonates;
- Inception of shortening during the Miocene. Here we assume that shortening propagated first to the southern margin of the basinal setting, and that each structure nucleated at the first thrust fold structure at the location of the former slope, as observed analogue models (Grelaud et al., 2002, for the Salt Range/Potwar Basin in Pakistan, Letouzey et al., 1995, for salt basins in general);
- Late inversion of the tilted fault blocks, associated with a marked propagation of the shortening and the main episode of folding and thrusting in the frontal belt.

4. Modelling results

4.1. Temperature and maturity calibration

The modelled temperature field is displayed in figure 8A. The comparison with well data provides a rather good fit. Temperatures from wells, using either Horner or WR corrections, have less than 10% mismatch on average, with the exception of the deep value at 2500m in the Bosavi well. Present day temperature gradients are also reproduced with a good match.

Another constraint is based on the temperature evolution of the Toro reservoir obtained from well data and core analysis: It should be close to 50°C at present day, and has never reached temperature higher than 90°C, as no quartz remobilization was observed. In addition, oil charge occurred after cooling below 50°C. The maximum temperature proposed by the modelling is 93°C, in accordance with fluid inclusion data, but the predicted present day

temperature is a bit too high and close to 63°C. This misfit may originate from two important effects: (1) an excessive surface temperature, but this should also increase local misfits in other wells; or (2) an underestimated cooling in the upper sedimentary section, due to the karstic surface water flow which is not taken into account in the modelling.

Most of the maturities recorded in the wells are closely matched (Figure 8B), as well as the maturity gradient at depth. This is particularly true for the Kanau-1 well, which is a major control point as it is also the locus of the most detailed AFTA study, where the erosional episode following Ieru sequence deposition was defined. A major discrepancy is observed in the Iagifu well, which shows a consistently higher maturity both at the contact between Darai and Ieru levels, and for the Toro sandstone reservoir. This is partly explained by a 300 m difference between the depth recorded in the well (top Toro at 2400 mMD) and the modelled geometry (top Toro at 2150 mMD), which will corresponds to a positive shift in maturity of 0.05%Ro, closer therefore to the observed values.

4.2 Porosity calibration

Porosity evolution is obtained through the use of porosity/depth curves from a standard basin simulator, during the back-stripping and decompaction process. This is done during the building of the kinematic scenario to rebuild the past geometry at each step of backstripping, taking the compaction into account. Based on the scenario, the highly porous zones are mainly the flexural basin deposits of Orubadi and Era beds due to their low amount of burial, together with the Toro sandstone reservoir at depth below the Darai Plateau and Hedinia area, where this horizon remains poorly compacted due to its low amount of burial.

By doing so, it appears that the porosity depth law for sandstones was nevertheless a bit too optimistic, thus predicting higher porosities than those observed. As a result, we have defined a new Toro lithology, which computes porosities at present day that are in good agreement with the well data. Average porosity at depth reaches more than 20 % in the shallow reservoirs from the Fly Platform to less than 13% in the Hedinia fold trend, consistent with the excellent hydrocarbon reservoirs.

4.3 Pressure calibration

This step is the most important one for the CERES2D fluid flow modelling, as the pressure gradients and hydraulic heads related to topography are the major cause of water flow. The dynamics of fluid circulation can be estimated only if the pressure field is representative of the real distribution of pressure. The predicted present day pressure field is shown on figure

9a. When comparing the predicted values to the observed ones, two major corrections were applied.

- First, one should determine what is the difference in burial between the real reservoir (Toro or Hedinia sandstone mostly) and the modelled one. A shift in depth of 100 m will correspond to an increase in pressure of 1 MPa (145 psi).
- A second major shift is due to the misfit in water table depth. The modelling assumes that the water table is at surface, whatever its elevation. If the observed water table is 500 m below the surface, the modelled hydrostatic pressure would be 5 MPa (725 psi) higher than the observed one.

For each well, elevation, formation tops and pressure (RFT data mostly) as well as water table depth (if observed) were used to compute the misfits.

The Bujon 1 (Figure 9b) well shows a Toro at 13.8 MPa, at 1400 mss, with a total burial of 1465 m. The modelled Toro is at 15.5 MPa, but with a present day elevation of 350 m, a depth of 1150 mss, and a burial of 1500 m. The water table shift is similar (30 m) and the pressure correction is then of 0.3+0.35=0.70M Pa. The misfit is then reduced to 1.3 MPa between the predicted and observed pressure. The modelling proposes a hydrostatic trend similar to the one observed.

The Kanau 1 well (Figure 9c) did not encounter a water table in the Darai Limestone. Therefore, we assume it is currently at the contact between the karstified carbonates and the Ieru Shale. The Toro reservoir at 370m sub-sea shows a 3.9 MPa pressure, at a total burial depth of 1330m. The Hedinia reservoir shows a 6.3 MPa pressure at 576m sub-sea. The same Toro horizon is at 1300m of burial in the modelled section, implying there is no correction of reservoir depth to apply there, with a predicted pressure of 7.2 MPa. The proposed water table at 400m sub-sea corresponds to a pressure shift of -4 MPa, which allows for a residual pressure of 7.2-4=3.2 MPa, close to the 3.9 MPa measured pressure. Taking into account the postulated water table depth, the modelled trend of pressure with depth can match the data points with a drop of pressure below the hydrostatic trend within the Ieru Shale.

The Bosavi-1 well (Figure 9d) has an elevation of 840masl, and shows a Toro reservoir at 300 mss and 3.7 MPa with a total burial of ~1100 m. The water table at 150m below the Ieru/Darai contact is poorly constrained. The modelled Toro is at 700 mss at 11.5 MPa, with a burial of 1300 m. The shift in the Toro burial corresponds to a 2 MPa correction, and the water table shift to a correction of 6 MPa. Thus the corrected pressure from the modeling is 3.5 MPa, close to the observed one. Again the three data points can be properly matched by the pressure trend obtained from the modelling and corrected.

The Iorogabaiu-1 well (Figure 8e) shows a Toro reservoir at 16.2 MPa at 1600 mss, with a total burial of 2200m (RT elevation of 640 masl). The modelled Toro gives a 24 MPa pressure at 2400 m of burial (practically hydrostatic). The corrected pressure output is thus 22 MPa. The aquifer is not observed but postulated at roughly 200 mss (middle part of the Darai limestone), which is compatible with both a hydrostatic trend, and a shift of the predicted pressure by 600 m or 6 MPa to fit the observed values.

The Hedinia structure is the most interesting one. The modelling output is a single well, but it can be compared to at least two real wells, Hedinia 1X (Figure 9f) and Hedinia 3X (Figure 9g). Hedinia 1X has an elevation of 1120 masl, and a water table at 370 masl. The Toro reservoir is encountered at 880 mss at 13.8 MPa, with a burial depth of 2000 m. The modelled Toro is at 900 mss, at a burial depth of 2100 m, and 15 MPa. The predicted pressure is effectively fitted if one takes into account the burial shift of 1 MPa, but is apparently above the hydrostatic value considering the water table depth. Thus it is not possible to fit the data point with the predicted pressure trend. Hedinia 3X has an elevation of 950 masl, and the Toro reservoir there is found at 1000 mss (burial of 2000 m) at a pressure of 13.8 MPa. The pressure correction due to burial is then of 1 MPa. Contrarily with Hedinia 1X, the water table is found at 900 masl, which corresponds to a correction due to water table shift of less than 1 MPa. Therefore, the fit is almost perfect, the three data points being in agreement with the predicted trend of pressure at depth. The pressure drop within the Ieru Shale allows connecting the hydrostatic trend in the upper layers to the mild under-pressure values observed below the Ieru Shale. It is important to note that the pressure appears regionally consistent in the structures below the shale, based on the two wells Hedinia-1X and Hedinia-2X which are similar. The major difference in the fitting is the water table depth, and we suspect that Hedinia-1X well encountered a deep karst network connected to the base of the carbonate.

Results from the Iagifu well (Figure 9h) are quite different between the model and the reality because the modelled well passes across a fault. The real well has an elevation of 1200masl, a water table at 915masl. The Toro reservoir is encountered at 2400 mBRT, at 15.1 MPa. A good fit was obtained between the under-pressurization trend and the three data points.

The Kutubu anticline is the only data point which is definitively not fitted (Figure 8i). The well elevation is at 1200masl with a water table at 800 masl. The Toro reservoir is found highly over-pressured at 40 MPa at 800 mbsl. The proposed pressure is again slightly under-pressured at 16 MPa at 650 mbsl.

The main conclusions of the pressure calibration are as follows

- Real hydrostatic trend occurs in the foreland,
- Within the Darai Plateau and the Hedinia, Iagifu, Zongwe and Iorogabaiu structures, there is a shifted hydrostatic trend, with pressures that are below hydrostatic values beneath the Ieru Shale.
- A shift of the water table by 300-700 m is possible (data in review):
- CERES2D is water saturated up to the surface, which is not the case in reality. The shift in pressure values in most wells can thus be explained firstly by a simple shift in the top of formation between the virtual well and the real one, and secondly by a shift in the water table (100m will equal 1MPa) in the karstified limestones
- Underpressurization below the Ieru Shale: A suction effect explained by the important flow of water from the summit of the anticlines toward adjacent topographical lows, onto the impervious shales. Such underpressurization has already been observed in other similar settings (Canadian Rocky Mountains, Colombian and Bolivian sub-Andean zones, Roure et al., 2003; Faure et al., 2004; Toro et al., 2004), and clearly reproduced by simple numerical experiments.
- No overpressurization is simulated in the Kutubu anticline, even if taking into account capillary effects for the seal, or decreasing the porosity/depth laws to diminish the porosity at a given depth, or increasing by two order of magnitude the specific surface (so decreasing in the same range the permeabilities). This implies that the overpressurization in the Kutubu field requires another explanation.

The major conclusion is that the modelling of pressure is able to predict quantitatively the pore fluid pressure values and trends if one takes into account the correction of reservoir depth and of water table level. The pressure prediction is, in contrast, not possible along the high pressure trend of the Kutubu anticline.

5 Petroleum system modelling

5.1 Source rock potential and characteristics

Oil discoveries in PNG, particularly those in the foldbelt trend were examined by Chevron following the discovery of oil and gas during the late 80's and early 1990's. Key studies include those of Moldowan and Lee (1987), Ahmed et al. (1988) and Kaufman (1994) and

they are the source of the following summary. This discussion refers to the commercial fields, which includes the Iagifu, Hedinia, Gobe and SE Gobe oil fields.

Light oil, condensate and gases obtained from seeps and subsurface reservoirs in PNG are genetically similar and have hydrocarbon compositions that are typically associated with generation from Type II/III to Type III kerogens. Based on the available geochemistry and rock extract data the source rock contains a mixture of marine and terrestrial organic matter deposited under mildly oxygenated conditions probably in an open marine to deltaic environment. The likely source rocks are of Jurassic age and show good to marginal potential and are comparable in organic facies and petroleum potential to the other Upper Jurassic source rocks present on the Northwest Shelf of Australia.

In the oil and gas fields in the PNG fold belt, rich source is not generally intersected in wells, however zones with marginal source potential are identified within the Upper Jurassic which contain low to moderate quantities of Type II/III to Type III (mixed marine and terrestrial) organic matter. These organic constituents will produce a mixture of oil and gas when mature with a concept that the source rock improves in richness into a basinal deep called the Kubor Kitchen thought to be the likely source of fold belt hydrocarbons, although local burial due to overthrusting is also a plausible charge model (Kaufman et al. 1994). The formation responsible is believed to be the Upper Jurassic Imburu Formation, with some potential in the Lower Jurassic (Chevron 1990, Waples and Wulff 1996). The Late Jurassic as a source rock concept is supported by oil – source correlations, demonstrating that the oils and source rocks are genetically similar (Moldowan and Lee, 1987).

In addition to the commercial fields, two other oil systems have been identified in the Papuan Basin. These include a distinctive Tertiary oil source as well as a probable Cretaceous oil source. The source rocks for these systems are poorly understood and are largely inferred from biomarker and isotopic evidence from the oils (Kaufman, 1994).

5.2 Maturity distribution and evolution

Figure 10 shows the present day distribution of the transformation ratio, which marks the maturation of the source rocks. This maturation is dependent upon the activation energy coefficient used to compute the thermal cracking of the organic matter. For that purpose, two types of source rocks have been used: (1) Marine type II source for the Lower Cretaceous and Upper Jurassic shale layers occurring between the reservoirs horizons, and (2) Continental type III source rock for the coal measures in the Lower Jurassic synrift deposits.

For each source rock, maturation starts in the Mid Cretaceous (Barremian). Maturation is mostly acquired in two steps: first during the regular burial in the Upper Cretaceous and Lower Tertiary, secondly due to the rapid burial in the foreland and below tectonic slices during compressional deformation (Upper Miocene to present day).

Synrift sequence are not mature below the Darai plateau, but their maturities below the tectonic units can reach 12% in the frontal slices, and up to 50% of transformation ratio below Mubi/Wage.

Modelling shows that for the Lower Cretaceous and Upper Jurassic source rocks half is the maturity was acquired during Mio-Pliocene time. Below Mubi, it reached 10% by late Oligocene, more than 25% in Late Miocene, and up to 50% for Lower Cretaceous source, 60% for Upper Jurassic at Present Day. Below the Darai plateau, it evolves from 2-6% by Late Oligocene, 5-12% for Late Miocene, and at present day reaches less than 10% in the Lower Cretaceous, 16-20% for Upper Jurassic. In most places, the Upper Jurassic source rock has the highest maturity due to its low activation energy distribution typical of type-II source rock, and highest thermal/burial history. Note that if we only consider type III source, the only location where the expulsion saturation will be obtained is the Mubi Wage zone.

5.3 Overall pattern of oil and gas migration and accumulation

To simulate oil and gas migration from the source rocks, viscosity, TOC and expulsion saturation have to be defined. A law regarding the temperature parameter describes the viscosity of oil, which is around 5 cP at surface conditions, corresponding to $5\ 10^{-3}$ Pa s. Similarly, a law regarding the temperature parameter describes the viscosity of gas, around 0.03 cP at surface conditions, corresponding to $3\ 10^{-5}$ Pa s.

The lithologies used in the modelling are defined by a mixture of sand and shale from pure lithologies. We changed the expulsion saturation parameters to the value of 5% for oil and 2% for gas, although the classic default value in the library of CERES2D was at a higher level (between 10 and 20%). We made this change to ease the migration process.

We used a total organic content of 1% for all the source rock layers present in the model. Indeed, the thickness of those layers is big, from 100m to 800m in the thickest parts. It corresponds to an average for the whole thick layer of a more realistic source rock layer that is inhomogeneous: a few tens of meters thickness with a richer content that may reach 10% of organic matter.

A first direct simulation of hydrocarbon charge and pathways is based on the reference model (figure 11A), based on the calibrated scenario and three source rock layers (type II source in

the Upper Jurassic and Cretaceous, and type III source only in the Triassic and lower Jurassic synrift sequence). This model shows two major results: oil is largely produced and reaches high saturation in several accumulations after a rapid migration, whereas little gas is produced, apart from in the deepest core of the belt, with small ranges of migration leading to small, low saturation accumulations (Figs 11A). Oil accumulations are located principally in structural traps, namely the Hedinia and Kutubu anticlines, and the deep Mubi duplex, with secondary accumulation located in the core of the antiform backlimb of Kutubu and in the fold controlled by the initiation of the out of sequences thrust below the Zongwe slices. In theses accumulation, oil saturation ranges from 10 to more than 60%, indicating potential economic accumulation. In contrast, gas is mostly confined within the source rock layers and along the main carrier beds where it reached the expulsion saturation (Figure 11 B). There is no economic accumulation, although gas saturation is higher than 50% at the source rock level and adjacent carrier beds. This result is inconsistent with the known gas accumulation in the Hedinia area. In our case, a large amount of gas is produced but poorly migrated.

Adding layers of type II source rocks in the deep part of the basin (i.e. in the lower Jurassic) enhances slightly the amount of generated oil (Figure 11B), reaching up to 60% saturation in the main accumulation, but does not change at all the general pattern of oil distribution. On the contrary, it increases the gas migration ability through a better expulsion at saturation, allowing for a small increase of saturation levels in the carrier beds and traps, up to 5%. There is still no economic accumulation developed.

A last step of modelling (Figure 11C) introduces the ability of secondary cracking to occur by decreasing the activation energy for secondary cracking from 57 to 54 $Kcal.mol^{-1}$, keeping the Arrhenius coefficient at $3.10^{14}.s^{-1}$. By doing so, the gas saturation is practically doubled, and in the Kutubu anticline reaches up to 10%. Oil accumulation is slightly increased as an increase in gas content enhances oil flow. Nevertheless, there is still very little gas accumulation, which is inconsistent with the known distribution.

5.4 Hydrocarbon migration paths

Considering the hydrocarbon pathways, the flow scenario shows three major steps (Figure 12). During the Late Cretaceous, after the erosion of the Ieru shale level, the modelling shows an early expulsion at saturation in the deep source rock beds. As the Ceres numerical scheme is highly diffusive in case of two-phase fluid flow, the seals around the source are also highly saturated, despite a very low porosity. This is followed, during the deposition of the Darai

carbonates by an early lateral migration in the reservoirs as early as Eocene, and coherent with the medium temperature recorded at 60°C in the fluid inclusion (1 in figure 12).

During the early stages of flexure and development of the imbricated units of the Mt Castle-Mubi-Wage area (from 7 to 2 My), we note the onset of the main lateral escape of hydrocarbon from the basin as a squeegee fluid flow updip to the flexure foreland (2 in figure 12). Hydrocarbons are mostly trapped in the early-formed Hedinia anticline (3 in figure 12). This prevents charge of the Darai plateau (4, 7 and 8 in figure 12). At the same time, oil is also trapped below the Mt Castle area.

In the late stages of fold and thrust belt evolution (2 My to present day) the main hydrocarbon migration occurs toward the upper part of the Darai plateau and into the Kutubu structure (5 and 6 in figure 12), toward the northernmost units in the Wage zone (5 in figure 12), and in the Darai plateau unit corresponding to the Zongwe slices, and deeper folds (8 in figure 12).

Migration velocities are quite small, ranging from 10 to 10^3 m.My^{-1} ()which is in the range of typical values between 20 to 300 m.My^{-1} (see Roure et al., 2010; Vilasi et al., 2009; Schneider et al., 2002), but on the low side, precluding long range migration paths owing to the age of migration inception at less than 4 Ma. The longest migration range would be no more than five kilometres.

7 Conclusions

The basin modeling CERES2D tool has been used to propose a valid scenario of hydrocarbon generation, migration and trapping within the Papua New Guinea fold and thrust belt, based on a 120km long balanced cross-section and 9 wells. Present day temperature, pore fluid pressure and maturity are well fitted apart from the high-pressure trend of the Kutubu anticline. Modelling results suggest a recent (i.e. less than 7My) maximum maturity with a short-range migration from the Cretaceous, Upper Jurassic and Triassic known source rock levels. Modelling results account for the know oil accumulation and potential migration pathways, but gas charge cannot be accounted for except by considering a second deep sediment accumulation below the main gas accumulation. Such a postulated Hedinia Trough, similar to the Swan graben in the Vulcan sub basin would help to produce larger amount of gas if secondary cracking of migrated oil occurs, with a short distance of migration. The high pressure trend, associated with an early charge and breaching of the anticline, is explained by taking into account a greater extent of the imbricate belt, which buried the Kutubu structural trend after its early charge and breaching, allowing for (1) the rebuilding of the sealing

capacity through clay diagenesis, and (2) for high pressure to build up at depth. Late, out of sequence reactivation of the trend explains the present day high pressure which is not yet re-equilibrated.

Acknowledgements

This paper is published with the permission of Oil Search Ltd, and IFP Energies Nouvelles.

References

1. Aitchinson J. C., Ireland T. R., Blake M. C. JR and Flood P. G. 1992. 530 Ma zircon age for ophiolite from the New England Orogen: oldest rocks known from eastern Australia. Geology, v. 20, 125–128.
2. Bessis, F., Burrus, J., Chenet, P.Y., Doligez, B., Lafargue, E., Ungerer, P. et al., 1987, A 2D model of basin-scale petroleum migration by two-phase fluid flow: Application to some case studies, in Doligez, B., ed., Migration of hydrocarbons in sedimentary basins. 3rd IFP Exploration and Production Research Conference, Carcans, June 15-19, 1987, Editions Technip, Paris.
3. Bessis, F., Burrus, J., Chenet, P.Y., Doligez, B. and Ungerer, P., 1990, Basin evaluation by integrated two-dimensional modelling of heat transfer, fluid flow, hydrocarbon generation and migration: AAPG Bull., v.74, 3, p.309-335.
4. Bodri, B., and L. Rybach (1998), Influence of topographically driven convection on heat flow in the Swiss Alps: A model study, Tectonophysics, 291, 19 – 27, doi:10.1016/S0040-1951(98)00028-6.
5. Bradey, K., Hill, K.C., Lund, D., Williams, N., Kivior, T., and Wilson, N. 2008. Exploration of the Kutubu oil field, Papua New Guinea. Geological Society of London Special Conference 'Fold and Thrust Belt', May 2008, London.
6. Bretan P., Yielding G., and Jones H., 2003. Using calibrated shale gouge ratio to estimate hydrocarbon column heights, Am. Ass. Petrol. Geol. Bull., 87, 397–413.
7. Brown A., 2003. Capillary effects on fault-fill sealing. Am. Ass. Petrol. Geol. Bull., 87, 381 395.
8. Burrus J., Kuhfuss A., Doligez B. and Ungerer P., 1991. Are numerical models useful in reconstructing the migration of hydrocarbons? A discussion based on the Northern

Viking Graben. In England W.A. and Fleet, A.J. (eds.) Petroleum Migration, Geol. Soc. Spec. Pub. 59, 89-109.

9. Burrus J., 1997. Contribution à l'étude du fonctionnement des systèmes pétroliers: apport d'une modélisation bidimensionnelle. Tome 1 et 2, thèse de l'Ecole des Mines de Paris, 346pp.
10. Callot, JP, Breesch, L., Roure, F., and Vilasi N., 2010. Paleo-fluids characterization and fluid flow modelling along a regional transect in the Northern UAE. Arabian Journal of Geosciences, 3, 413-437, doi.10.1007/s12517-010-0233-z.
11. Carman G.J. And Z., (Eds) 1990, Petroleum Exploration and Development in Papua New Guinea; Proceedings of the First PNG Petroleum Convention, Port Moresby, 12-14th February, 1990, 597pp.
12. Carman G.J. And Z., (Eds) 1993, Petroleum Exploration and Development in Papua New Guinea; Proceedings of the 2nd PNG Petroleum Convention, Port Moresby, 31st May-2nd June, 1993, 688pp.
13. Chenet, P.Y., Doligez, B. and Schmerber, G., 1986, The Themis model: a new tool for the hydrocarbon exploration: Integrated study of the sedimentary basin from the sedimentation to the hydrocarbon accumulation: Hidrocarburos, 1° Congreso Latino-Americano, Buenos Aires, 4-11 de Mayo 1986, v.10, p.5187-5202.
14. Cole J. P., Parish M. and Schmidt D. 2000. Sub-thrust plays in the Papuan Fold Belt: the next generation of exploration targets. In: Buchanan P. G., Grainge A. M. and Thornton R. C. N. eds. Papua New Guinea's Petroleum Industry in the 21st Century, Proceedings of the 4th PNG Petroleum Convention, pp. 87–100. Papua New Guinea Chamber of Mines, Port Moresby.
15. Cooper, G.T., Hill, K.C., and Baxter, K., 1996. Rifting in the Timor Sea and New Guinea: A template for compressional forward modeling. In: Buchana, P.G. (Eds.) Petroleum Exploration, Development and Production in Papua New Guinea. Proceed. Third PNG Petrol. Conv., Port Moresby, 133-144.
16. Corbett G. J. 1994. Regional structural control of selected Cu/Au occurrences in Papua New Guinea. In: Rogerson R. ed. Proceedings of the PNG Geology, Mining and Exploration Conference 1994, pp. 57–70. Australasian Institute of Mining and Metallurgy, Melbourne.
17. Crowhurst P. V. 1999. The tectonic history of northern Papua New Guinea. PhD thesis, La Trobe University, Melbourne (unpubl.).

18. Deville, E. and Sassi, W., 2006, Contrasting thermal evolution of thrust systems: an analytical and modelling approach in the front of the Western Alps: AAPG Bull., v.90, 6, p.887-907.
19. Divies, R. and Sassi, W., 1996, Foldis: forward modelling of folding and compaction: Annales Geophysicae, 14, 1, C106.
20. Doligez, B., ed., 1987, Migration of hydrocarbons in sedimentary basins: 3rd IFP Exploration and Production Research Conference, Carcans, June 15-19, 1987, Editions Technip, Paris, 712 pp.
21. Duddy, I.R., Marshallsea, S.J. and Arne, D.C. 1991. The Papuan Basin regional thermal and maturation analysis incorporating apatite fission track analysis of twenty seven wells with emphasis on the relative timing and hydrocarbon maturity and kerogen kinetic typing of source rock. Geotrack report 232, 110pp.
22. England W.A., MacKenzie A.S., Mann D.M., and Kingley T.M., 1987. The movement and entrapment of petroleum fluids in the subsurface. J. Geol. Soc. London, 144, 327-347.
23. Faille, I., Nataf, F., Schneider, F. and Willien, F., 1998, Domain decomposition methods for fluid flows in porous medium: ECMOR, 6th European Conference on the Mathematics of Oil Recovery, Peebles, September 8-11, 1998, Proceedings, Paper B-06, 6pp.
24. Faure J.L., Osadetz K., Benaouali N., Schneider F., and Roure F., 2004. Kinetic and petroleum modelling of the Alberta foothills and adjacent foreland - West of Calgary. Rev. Inst. Fr. Petrol., 59, 81-108.
25. Ferket, H., Roure, F., Swennen, R. and Ortuño, S., 2000, Fluid migration placed into the deformation history of fold-and-thrust belts: an example from the Veracruz Basin (Mexico): Journal of Geochemical Exploration, v.69-70, p.275-279.
26. Ferket, H., 2006, Kinematic evolution, diagenesis and fluid flow reconstruction in the Laramide fold-and-thrust belt of eastern Mexico (Córdoba Platform and Veracruz Basin): implications for petroleum exploration: Inst. Mex. Petr. and Inst. Frac. Petr., IFP report, 123 pp.
27. Forster, C., and L. Smith (1989), The influence of groundwater flow on thermal regimes in mountainous terrain: A model study, J. Geophys. Res., 94, 9439 – 9451, doi:10.1029/JB094iB07p09439.
28. Gonzalez, E., Ferket, H., Callot, J.P., Guilhaumou N., Ortuno, F., Roure, F. 2013. Paleoburial, hydrocarbon generation and migration in the Cordoba platform and

869 Veracruz basin: Insights from fluid inclusion studies and 2D-modelling. SEPM
870 Special Publication 11, ISBN 978-1-56576-315-9, p. 167–186.
871 29. Green, P.F., 2001. Thermal history reconstruction in PNG well Kanau-1, using AFTA
872 and Vitrinite reflectance. Geotrack report 820, 95pp.
873 30. Hardebol, N., Callot, J.P., Bertotti, G., Faure, JL., 2009. Sedimentary and Tectonic
874 Burial history appraisal and consequent Temperature and Organic Maturation
875 evolution in thrust-belt systems: a study on the SE Canadian Cordillera. Tectonics, 28,
876 TC3003, doi:10.1029/2008TC002335.
877 31. Henry, P., and Wang, C.Y., 1991. Modelling of fluid flow and pore pressure at the toe
878 of Oregon and Barbados accretionnary wedges. J. Geophys. Res., 96, 20109-20130.
879 32. Hill K. C., Simpson R. J., Kendrick R. D., Crowhurst P. V., O'Sullivan P. B. and
880 Saefudin I. 1996. Hydrocarbons in New Guinea, controlled by basement fabric,
881 Mesozoic extension and Tertiary convergent margin tectonics. In: Buchanan P. G. ed.
882 Petroleum Exploration, Development and Production in Papua New Guinea,
883 Proceedings of the 3rd PNG Petroleum Convention, Port Moresby, pp. 63–76. Papua
884 New Guinea Chamber of Mines, Port Moresby.
885 33. Hill K. C. and Raza A. 1999. Arc–continent collision in Papua Guinea: constraints
886 from fission track thermochronology. Tectonics 18, 950–966.
887 34. Hill, K.C., and Hall, R. 2002. Mesozoic-Cenozoic evolution of Australia's New
888 Guinea margin in a west Pacific context. Geol. Soc. Austral. Spec. Pub., 22, 259-283.
889 35. Hill, K.C., Iwanec, J., Bradey, K. and Wilson, N., 2008. Crustal architecture, fold belt
890 development and oil field compartments in Papua New Guinea. Geological Society of
891 London Special Conference 'Fold and Thrust Belt', May 2008, London.
892 36. Hill, K.C., Callot, J.P., Parish, M., Wood, S., Bradey, K., and Roure, F., 2010.
893 Structural development and hydrocarbon charge of the Kutubu oil and field, PNG.
894 ASEG/PESA meeting.
895 37. Husson, L., and I. Moretti (2002), Thermal regime of fold and thrust belts – an
896 application to the Bolivian sub-Andean zone, Tectonophysics, 345, 253 – 280,
897 doi:10.1016/S0040-1951(01)00216-5.
898 38. Longley, I.M., Buessenschuett, C., Clydsdale, L., Cubitt, C.J., Davis, R.C., Johnson,
899 M.K., Marshall, M.N., Murray, A.P., Somerville, R., Spry, T.B., and Thompson, N.B.,
900 2002. The North West Shelf of Australia – A Woodside perspective. In Keep, M. and
901 Moss, S.J. (Eds.) The Sedimentary Basins of Western Australia 3. Proceed. Petrol.
902 Explor. Soc. Austral. Symp., Perth, 27-88/

39. Machel, H. G. and Cavell, P.A.,1999. Low-flux, tectonically-induced squeegee fluid flow ("hot flash") into the Rocky Mountain foreland basin. Bull. Canadian Petrol. Geol., 47, 510-533.
40. Metcalfe I. 1996. Pre-Cretaceous evolution of SE Asian terranes. In: Hall R. and Blundell D. J. eds. Tectonic Evolution of SE Asia, pp. 97–122. Geological Society of London Special Publication 106.
41. Rogerson R. J., Hilyard D., Finlayson E. J., Holland D. S., Nion S. T. S., Sumaiang R. S., Duguman J. and Loxton C. D. C. 1987. The geology and mineral reserves of the Sepik headwaters region, Papua New Guinea. Geological Survey of Papua New Guinea Memoir 12.
42. Osadetz, K., B. Kohn, S. Feinstein, and R. Price (2004), Deformation, fluid flow and reservoir appraisal, in Foreland fold and thrust belts, in Deformation, Fluid Flow, and Reservoir Appraisal in Foreland Fold and Thrust Belts, AAPG Hedberg Ser., vol. 1, edited by R. Swennen, F. Roure, and J. W. Granath, pp. 21 – 48, Am. Assoc. of Pet. Geol., Tulsa, Oklahoma
43. Oliver, J. (1986) Fluids Expelled Tectonically from Orogenic Belts: their Role in Hydrocarbon Migration and Other Geological Phenomena. Geology, 14, 99-102.
44. Roure, F., 2008, Foreland and hinterland basins: What controls their evolution?: Davos Proceedings, Swiss Journal of Earth Sciences, Birkhaüser Verlag, Basel, doi: 10.1007/s00015-008-1285-x.
45. Roure, F., H. Alzaga, JP. Callot, H. Ferket, D. Granjeon, E. Gonzalez, N. Guilhaumou, M. Lopez, P. Mougin, S. Ortuno and M. Séranne, 2009. Long lasting interactions between tectonic loading, unroofing, post-rift thermal subsidence and sedimentary transfers along the western margin of the Gulf of Mexico: Some insights from integrated quantitative studies. Tectonophysics, 475, 169-189.
46. Roure F., Andriessen, P., Callot J.P., Ferket H., Gonzales E., Guilhaumou N. Lacombe O., Malandain J., Mougin P., Swennen R. and Vilasi N., 2010. The use of paleo-thermo-barometers and coupled thermal, fluid flow and pore fluid pressure modeling for hydrocarbon and reservoir prediction in fold and thrust belts. Geol. Soc. London Spec. Pub., 348, 87-114, doi:10.1144/SP348.6.
47. Roure, F., Swennen, R., Schneider, F., Faure, J.L., Ferket, H., Guilhaumou, N., Osadetz, K., Robion, P. and Vandeginste, V., 2005, Incidence and importance of tectonics and natural fluid migration on reservoir evolution in foreland fold-and-thrust belts: Oil and Gas Sci. and Tech., Rev. IFP, v.60, 1, p.67-106.

48. Sassi, W. and Rudkiewicz, J. L., 1999, THRUSPACK Version 6.2: 2D Integrated maturity studies in thrust areas: IFP report, 45372.
49. Saffer, D.M., and Bekins, B.A., 1998. Episodic fluid flow budget in the Nankai accretionnary complex: timescale, geochemistry, flow rates and fluid budget. J. Geophys. Res., 103, 30351-30370.
50. Schneider, F., Devoitine, H., Faille, I., Flauraud, E. and Willien, F., 2002, Ceres2D: A numerical prototype for HC potential evaluation in complex area: Oil and Gas Science and Technology, Rev. IFP, v.57, 6, p.607-619.
51. Schneider, F., 2003, Basin modelling in complex are: Examples from Eastern Venezuelan and Canadian foothills: Oil and Gas Science and Technology, Revue de l'IFP, v.58, 2, p.313-324.
52. Schneider, F., Pagel, M. and Hernandez, E. 2004, Basin modelling in complex area: Example from Eastern Venezuelan Foothills, in Swennen, R., Roure, F. and Granath, J., eds., Deformation, fluid flow and seservoir appraisal in foreland fold and thrust belts, AAPG Hedberg Mem., v.1.
53. Skarbek, R.M. and Saffer, D.M. 2009. Pore pressure development beneath the decollement at the Nankai subduction zone: Implications for plate boundary fault strength and sediment dewatering. J. Geophys. Res. doi:10.1029/2008JB006205.
54. Tobin, H.J., and Saffer, D.M., 2009. Elevated fluid pressure and extreme mechanical weakness of a palte boundary thrust, Nankai Trough subduction zone. Geology, 37, 679-682.
55. Ungerer, P., 1990, State of the art of research in kinetic modelling of oil formation and expulsion: Organic Geochemistry, Pergamon Press, Oxford, v.16, 1-3, p.1-25.
56. Ungerer, P., Burrus, J., Doligez, B., Chénet, PY., and Bessis, F., 1990. Basin evaluation by integrated two dimensional modelling of heat transfert, fluid flow, hydrocarbon generation and migration. Am. Assoc. Petrol. Geol. Bull., 74, 309-335.
57. Vilasi, N., Malandain, J., Barrier, L., Callot, J.P., Amrouch, K., Guilhaumou, N., Lacombe, O., Musqa, K., Roure, F., Swennen, R., 2009. From outcrop and petrographic studies to basin scale fluid flow modelling: The use of the Albanian natural laboratory for carbonate reservoir characterisation. Tectonophysics, 474, 367-392.
58. Wilson, N., Hill, K.C., Iwanec, J., Lund, D., Xu, K., Mann, P. and Bradey, P. 2008. Moran oil field PNG, A case study. Geological Society of London Special Conference 'Fold and Thrust Belt', May 2008, London.

Figure captions

Figure 1: A) Tectonic map of New Guinea and the southwest Pacific region with principal geographical locations referred to in the text. Barbed lines are active subduction zones and thick lines are active spreading centres. The light blue shaded areas, drawn at the 200 m isobath, are the continental shelves of Eurasia and Australia and areas of thickened oceanic crust/arcs. B) New Guinea showing simplified tectonic belts and the principal tectonic features. AB, Amanab Block; AR, Adelbert Ranges; BB, Bintuni Basin; BG, Bena Bena–Goroka Terrane; B–T, Bewani–Torricelli Mountains; CM, Cyclops Mountains; COB, Central Ophiolite Belt; DF, Derewo Fault; FR, Finisterre Ranges; G, Gauttier Terrane; GM, Grasberg mine; HG, Huon Gulf; HP, Huon Peninsula; In, Indenburg Inlier; K, Kubor Range; La, Landslip Ranges; LF, Lagaip Fault; MB, Meervlakte Basin; Po, Porgera Intrusive Complex and mine; RB, Ramu Basin; SB, Sepik Basin; SG, Strickland Gorge; ST, Sepik Terrane; Wa, Wandaman Peninsula; WT, Weyland Terrane. (from Hill and Hall 2002). C). Sun-shaded, digital elevation model showing the main features of the Papuan Fold Belt. The main structural belts are labelled, after APC (1961). The Darai Plateau is a very large asymmetric anticline overlying an inverted extensional fault that was active from Triassic to Miocene times. The structure is offset by a tear fault, the Bosavi Lineament, to underlie the mountain front in the NW part of the fold belt. All the producing oil and gas fields lie within the Strongly Folded Belt. Key wells are labelled and oil field and gas field outlines are shown in green and red, respectively. Wells within the fields are shown by white dots but, for clarity, are not labelled.

Figure 2: 3D sketch evolution of the paleogeography of New Guinea, from the Jurassic to present day structure, illustrating the role of the Tasman line in dividing New Guinea in two contrasted zones (from Hill and Hall, 2002). a) Jurassic; b) Cretaceous, from the subducting slab and accretionary prism to the Coral Sea rift; c) Paleogene, opening of the Coral Sea and denudation on the eastern Papua New Guinea; d) Oligocene, arrival of the Philippine Arc; e) Early Miocene, differentia subsidence with carbonates deposition in the South and exhumation of core complexes in the North; f) Mid Miocene; g) Pliocene arrival of the Carolina Arc and development of the fold belt above a weak hot plate; h) Pleistocene and basement reactivation, but still no foreland basin.

Figure 3A Simple chronostratigraphic chart for the New Guinea fold belt (after Hill and Hall, 2002). It shows the preserved Palaeozoic section west of the Tasman line, and the lower Mesozoic which is locally intruded to the east. Following the Jurassic break-up, the Mesozoic clastic succession is relatively homogeneous. The lower Tertiary uplift in the east led to an important unconformity below the Darai limestone, prior to the foreland basin clastic succession. B) Simplified stratigraphy across the Papuan Fold Belt (after Hill et al. 2000) flattened on the top Miocene. The Mesozoic section is dominantly mudstone, but contains the Upper Jurassic to Neocomian Iagifu, Hedinia, Digimu and Toro sandstone reservoirs. These are collectively modelled as Toro Sandstone. The Cretaceous Ieru Mudstone is the regional seal and is unconformably overlain by the thick Miocene Darai Limestone and Orubadi Marls. The Upper Triassic and Lower Jurassic syn-rift sequence is schematic on this section.

Figure 4: Present day balanced cross section modified from Hill et al. (2008). The closest wells used in the study have been shown, but the Iagifu-1s Usano-1 and Iorugabai-1 wells are not shown although used with a longer projection distance.

Figure 5A: Schematic workflow of the CERES2D tool used for modelling fluid flow in complex setting (e.g. Schneider et al., 2002; 2003). B: The four steps of the present days ection edition; a) editing the section geometry; b) editing the geological properties of the section; c) creation of he section topology (i.e. definition of the kinematic mobile blocks); dç building of the calculation grid for each block. C: Each restoration step comprises four steps repeated for each satge of evolution of the kinematic (i.e. at minimum each sedimentary layer): 1) edition of the eroded parts in the initial section, i.e. at the youngest age of the stage; 2) back-stripping of the layer deposited during the modelled stage; 3) kinematic restoration; 4) management of thicknesses discrepencies related to block adjustements.

Figure 6: Present day section used for the basin modelling phase, with the approximate location of the well used for the calibration process, together with the interpreted section from Hill et al. (2008).

Figure 7. Kinematic scenario based on the structural interpretation by Hill et al. (2008), assuming a weak lithosphere, roughly 1 km of erosion for the Ieru Shale, and an early activation of the frontal thrust fault limiting the Hedinia structure.

Figure 8A. Temperature calibration A1) Temperature distribution in the present day section. A2-7) Comparison between the predicted (continuous lines) and observed (dots, white for WR, red for Horner correction) temperatures at various calibration wells (depth in meter).
8B) Maturity calibration. B1) Distribution of maturity Comparison between the predicted (continuous lines) and observed (white dots) value of vitrinite reflectance at various calibration wells (depth in meters).

Figure 9. Calibration of the pressure distribution along the section. B1) Present-day distribution of pressure along the section. B2-9): Comparison between predicted (red line and squares with log on the right) and observed (white crosses and line with log on the left side) pressure data for the calibration wells. The blue lines correspond to the expected real trend, obtained by shifting the predicted trend after applying all corrections. The water table depth is here proposed at the contact between Darai carbonates and Ieru shales.

Figure 10: A) Distribution of transformation ration at present day and evolution with time for three main area; Evolution of the transformation ratio for the Darai plateau (B) Hedinia-Kutubu (C) and Mubi-Wage (D), for the three source rocks (Red: Lower Cretaceous, Green: Upper Jurassic, Blue, syn rifit coal sequence).

Figure 11: Oil and gas accumulations for various sets of simulation. A) reference model with three source rocks (Lower Cretaceous type II, Upper Jurassic type II, syn rifit coal sequence type III). B) Similar as previous model with a mixture of type II and III source rocks for the lower productive unit in the Triassic. C) Similar as previous model with secondary cracking enabled (see text for explanations).

Figure 12. Three steps of evolution of the hydraulic head (i.e. the piezometric high above the reference level, here in CERES2D the sea level), which expresses the potential energy driving fluid motion. Three time steps are represented, from bottom to top Top Darai (7Ma), Top Orubadi (5Ma), Present Day (0Ma). Arrows denotes oil velocity, the arrow size ranging from 1 to 50m/Ma. (1) Onset of lateral migration; (2) Main squeegee fluid flow episode; (3) early development of the Hedinia anticline charge; (4) Southward extent of the squeegee fluid flow, accumulation against the Darai plateau bounding fault; (5) Maximum oil and gas escape from the deep kitchen, charge of the inner Mubi and Wage zones; (6) Late emplacement of the Kutubu anticline with late oil charge, closure of the flow toward Hedinia; (7) beginning of oil

accumulation in the Darai plateau due to flexure; (8) beginning of oil charge in the Zongwe units.


(A) Tectonic Setting of New Guinea
PHILIPPINE SEA PLATE
Philippines
Mindanao
Halmahera
Bacan
Obi
Celebes Sea
Sulawesi
Bangai
Sula Islands
Banda Sea
CAROLINE PLATE
Caroline Ridge
PACIFIC PLATE
Ontong Java Plateau
New Guinea
Bismarck Sea
Solomon Sea
Woodlark Basin
Solomons
Coral Sea
Vitiaz Trench
Samoa
North Fiji Basin
Fiji
New Hebrides
New Caledonia
INDIAN-AUSTRALIAN PLATE
Australia
Tasman Line
Lord Howe Rise
South Fiji Basin
Tonga-Kermadec Arc
Tasman Sea
New Zealand
20°N
10°N
0°
10°S
20°S
30°S
120°E
130°E
140°E
150°E
160°E
170°E
180°E
190°E

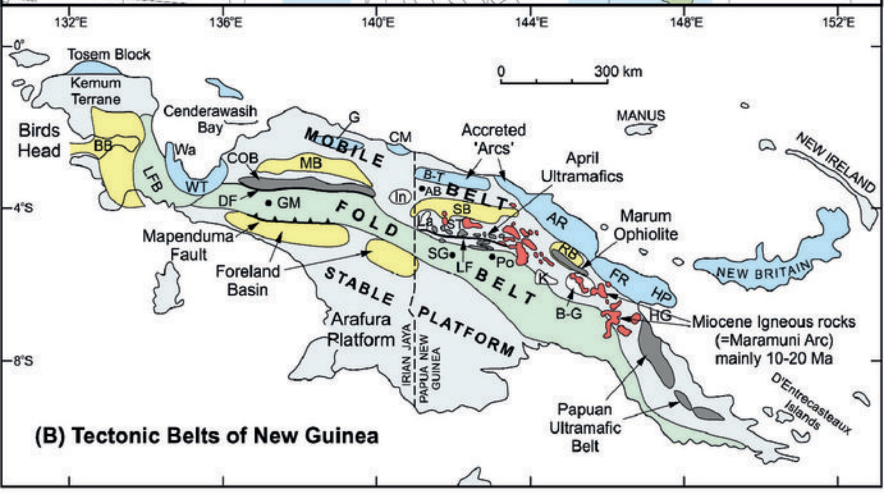
132°E
136°E
140°E
144°E
148°E
152°E
0°
4°S
8°S
0
300 km
Tosem Block
Kemum Terrane
Birds Head
BB
LFB
Cenderawasih Bay
Wa
WT
COB
DF
GM
G
MB
CM
MOBILE BELT
FOLD BELT
Accreted 'Arcs'
April Ultramafics
B-T
AB
In
SB
La
ST
SG
LF
Po
K
B-G
RB
AR
FR
HP
HG
Marum Ophiolite
MANUS
NEW IRELAND
NEW BRITAIN
Mapenduma Fault
Foreland Basin
STABLE PLATFORM
Arafura Platform
IRIAN JAYA
PAPUA NEW GUINEA
Miocene Igneous rocks (=Maramuni Arc) mainly 10-20 Ma
Papuan Ultramafic Belt
D'Entrecasteaux Islands
(B) Tectonic Belts of New Guinea

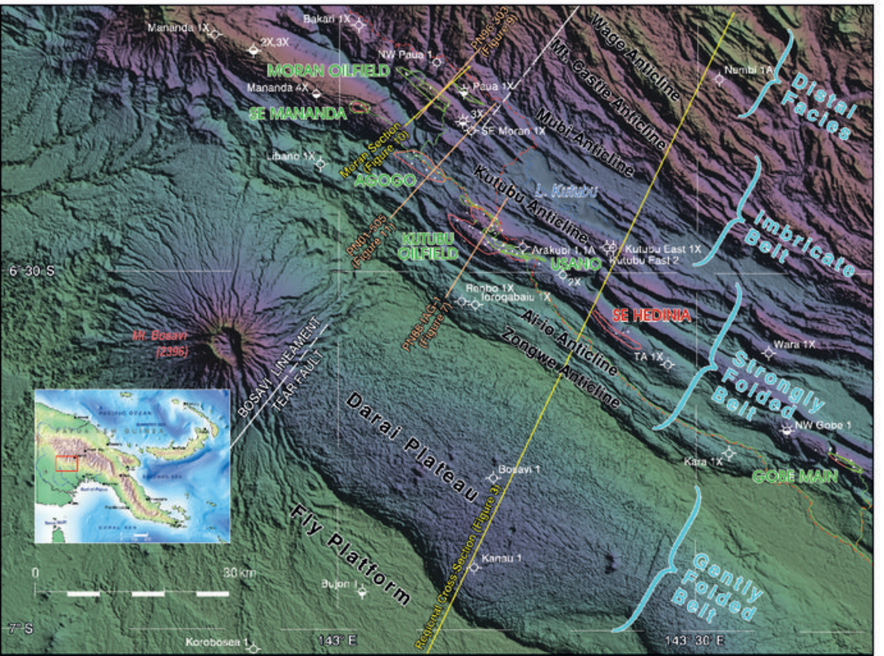
Mananda 1X
2X,3X
Bakari 1X
NW Paua 1
MORAN OILFIELD
Mananda 4X
Paua 1X
SE MANANDA
3X
SE Moran 1X
Moran Section (Figure 10)
Libano 1X
AGOGO
KUTUBU OILFIELD
Arakubi 1,1A
Kutubu East 1X
Kutubu East 2
USANO
2X
Ronbo 1X
Iorogaibau 1X
SE HEDINIA
TA 1X
Wage Anticline
Mt. Castle Anticline
Mubi Anticline
Kutubu Anticline
L. Kutubu
Ai-io Anticline
Zongwe Anticline
Numbi 1A
Distal Facies
Imbricate Belt
Strongly Folded Belt
Gently Folded Belt
Wara 1X
NW Gobe 1
Kara 1X
GOBE MAIN
6°30'S
7°S
143°E
143°30'E
Mt. Bosavi (2396)
BOSAVI LINEAMENT TEAR FAULT
Darai Plateau
Fly Platform
Bosavi 1
Kanau 1
Bujon 1
Korobosea 1
Regional Cross Section (Figure 3)
0
30 km

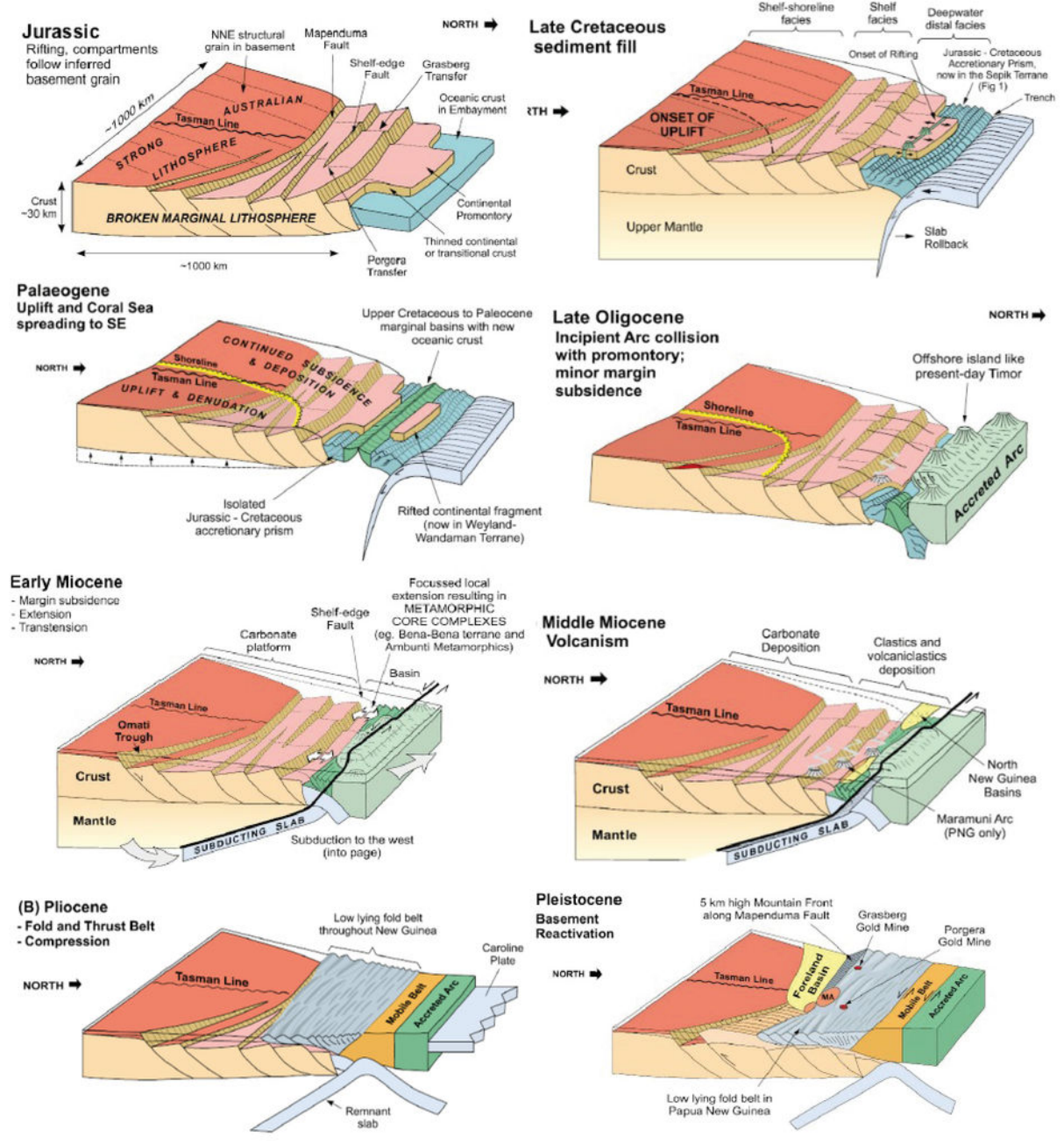
Jurassic
Rifting, compartments follow inferred basement grain
NNE structural grain in basement
Mapenduma Fault
NORTH
Shelf-edge Fault
Grasberg Transfer
Oceanic crust in Embayment
~1000 km
AUSTRALIAN
Tasman Line
STRONG
LITHOSPHERE
Crust ~30 km
BROKEN MARGINAL LITHOSPHERE
Continental Promontory
Thinned continental or transitional crust
~1000 km
Pergera Transfer
Late Cretaceous sediment fill
Shelf-shoreline facies
Shelf facies
Deepwater distal facies
Onset of Rifting
Jurassic - Cretaceous Accretionary Prism, now in the Sepik Terrane (Fig 1)
Trench
Tasman Line
ONSET OF UPLIFT
Crust
Upper Mantle
Slab Rollback
Palaeogene
Uplift and Coral Sea spreading to SE
NORTH
Upper Cretaceous to Paleocene marginal basins with new oceanic crust
CONTINUED SUBSIDENCE & DEPOSITION
Shoreline
Tasman Line
UPLIFT & DENUDATION
Isolated Jurassic - Cretaceous accretionary prism
Rifted continental fragment (now in Weyland-Wandaman Terrane)
Late Oligocene
Incipient Arc collision with promontory; minor margin subsidence
NORTH
Offshore island like present-day Timor
Shoreline
Tasman Line
Accreted Arc
Early Miocene
- Margin subsidence
- Extension
- Transtension
NORTH
Carbonate platform
Shelf-edge Fault
Focussed local extension resulting in METAMORPHIC CORE COMPLEXES (eg. Bena-Bena terrane and Ambunti Metamorphics)
Basin
Tasman Line
Omati Trough
Crust
Mantle
SUBDUCTING SLAB
Subduction to the west (into page)
Middle Miocene Volcanism
NORTH
Carbonate Deposition
Clastics and volcaniclastics deposition
Tasman Line
Crust
Mantle
SUBDUCTING SLAB
North New Guinea Basins
Maramuni Arc (PNG only)
(B) Pliocene
- Fold and Thrust Belt
- Compression
NORTH
Low lying fold belt throughout New Guinea
Caroline Plate
Tasman Line
Mobile Belt
Accreted Arc
Remnant slab
Pleistocene
Basement Reactivation
NORTH
5 km high Mountain Front along Mapenduma Fault
Grasberg Gold Mine
Porgera Gold Mine
Tasman Line
Foreland Basin
MA
Mobile Belt
Accreted Arc
Low lying fold belt in Papua New Guinea

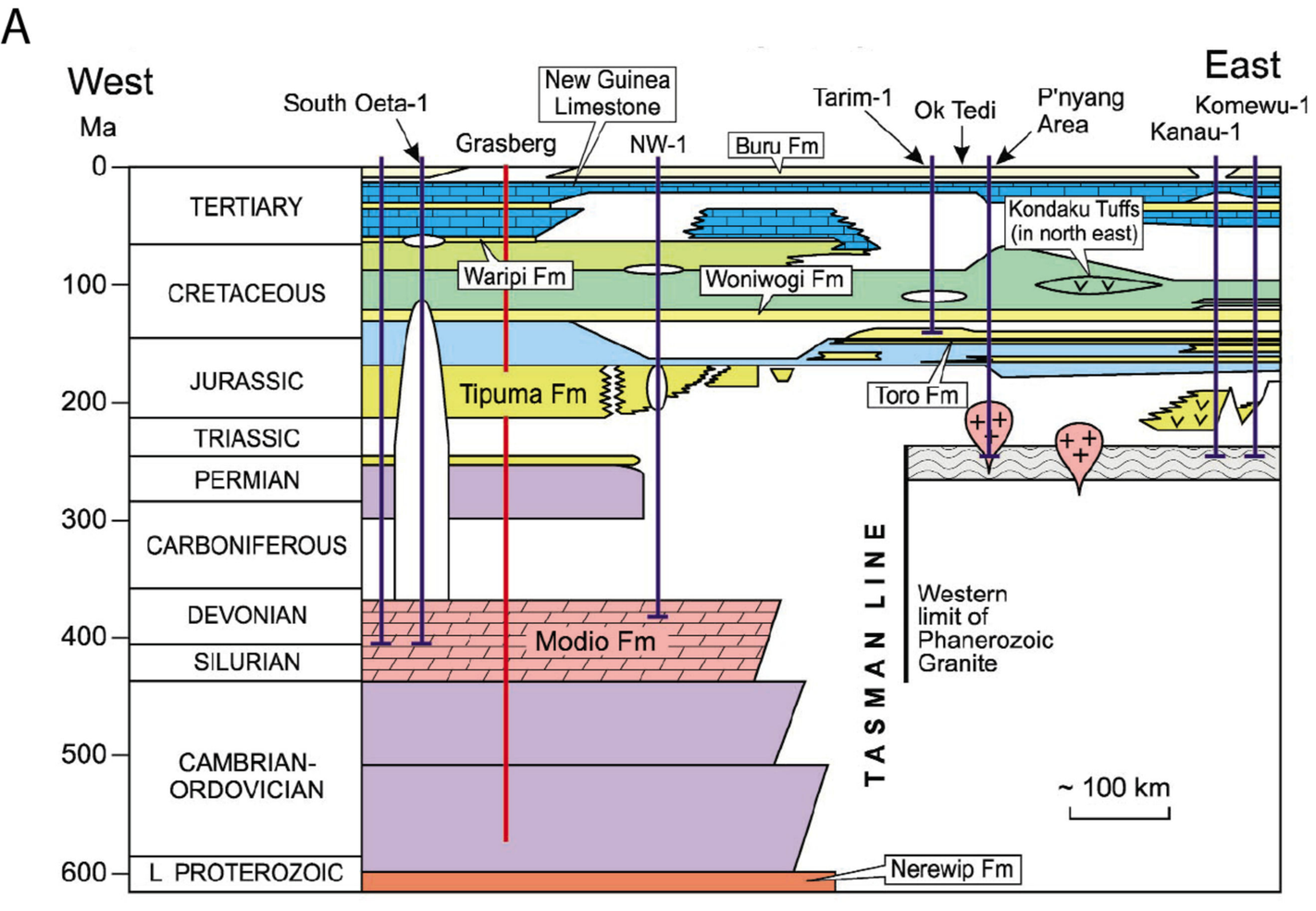
A
West
East
Ma
0
100
200
300
400
500
600
TERTIARY
CRETACEOUS
JURASSIC
TRIASSIC
PERMIAN
CARBONIFEROUS
DEVONIAN
SILURIAN
CAMBRIAN-
ORDOVICIAN
L PROTEROZOIC
South Oeta-1
Grasberg
New Guinea
Limestone
NW-1
Buru Fm
Tarim-1
Ok Tedi
P'nyang
Area
Komewu-1
Kanau-1
Kondaku Tuffs
(in north east)
Waripi Fm
Woniwogi Fm
Tipuma Fm
Toro Fm
Modio Fm
TASMAN LINE
Western
limit of
Phanerozoic
Granite
~ 100 km
Nerewip Fm

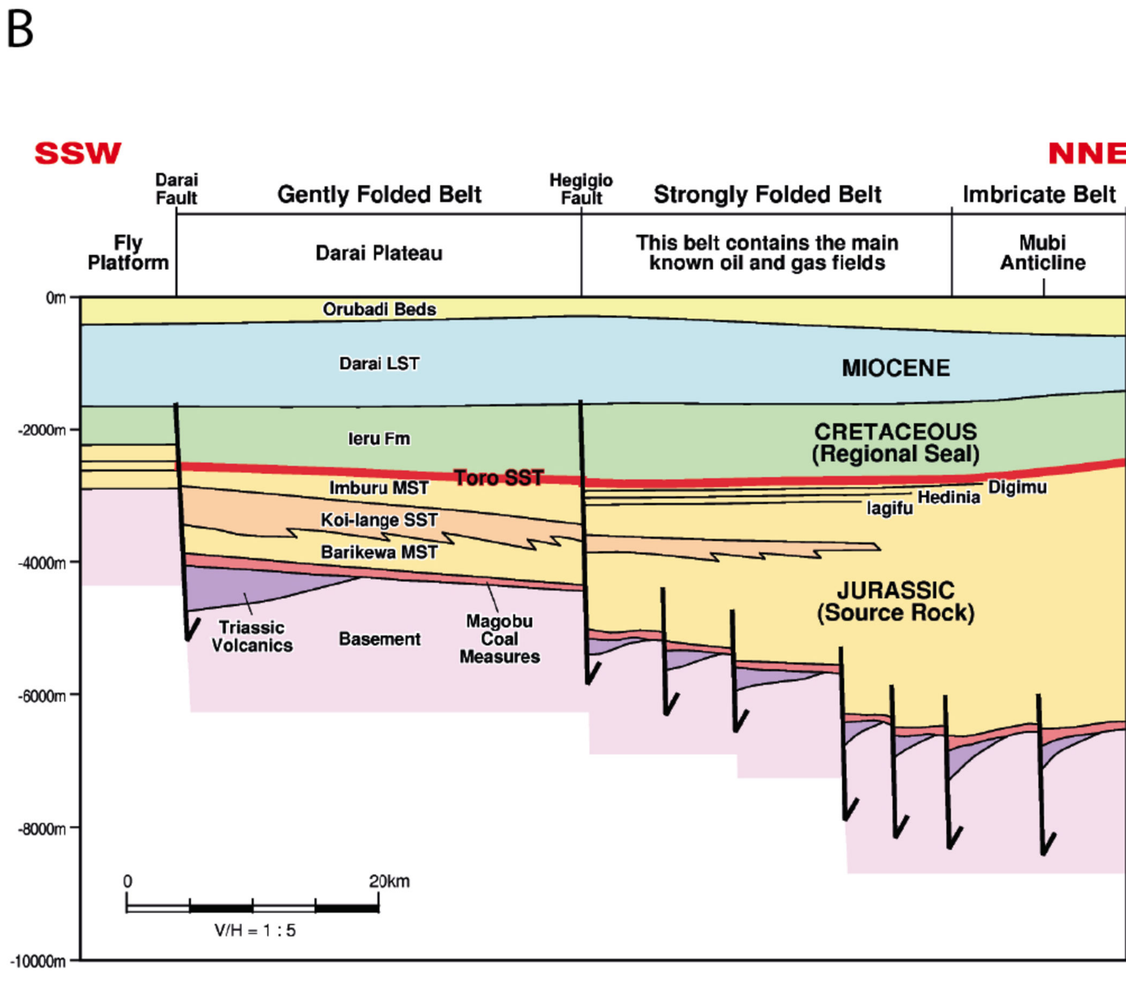
B
SSW
NNE
Darai
Fault
Gently Folded Belt
Hegigio
Fault
Strongly Folded Belt
Imbricate Belt
Fly
Platform
Darai Plateau
This belt contains the main
known oil and gas fields
Mubi
Anticline
0m
-2000m
-4000m
-6000m
-8000m
-10000m
Orubadi Beds
Darai LST
MIOCENE
Ieru Fm
CRETACEOUS
(Regional Seal)
Toro SST
Imburu MST
Koi-lange SST
Barikewa MST
Iagifu
Hedinia
Digimu
JURASSIC
(Source Rock)
Triassic
Volcanics
Basement
Magobu
Coal
Measures
0
20km
V/H = 1 : 5

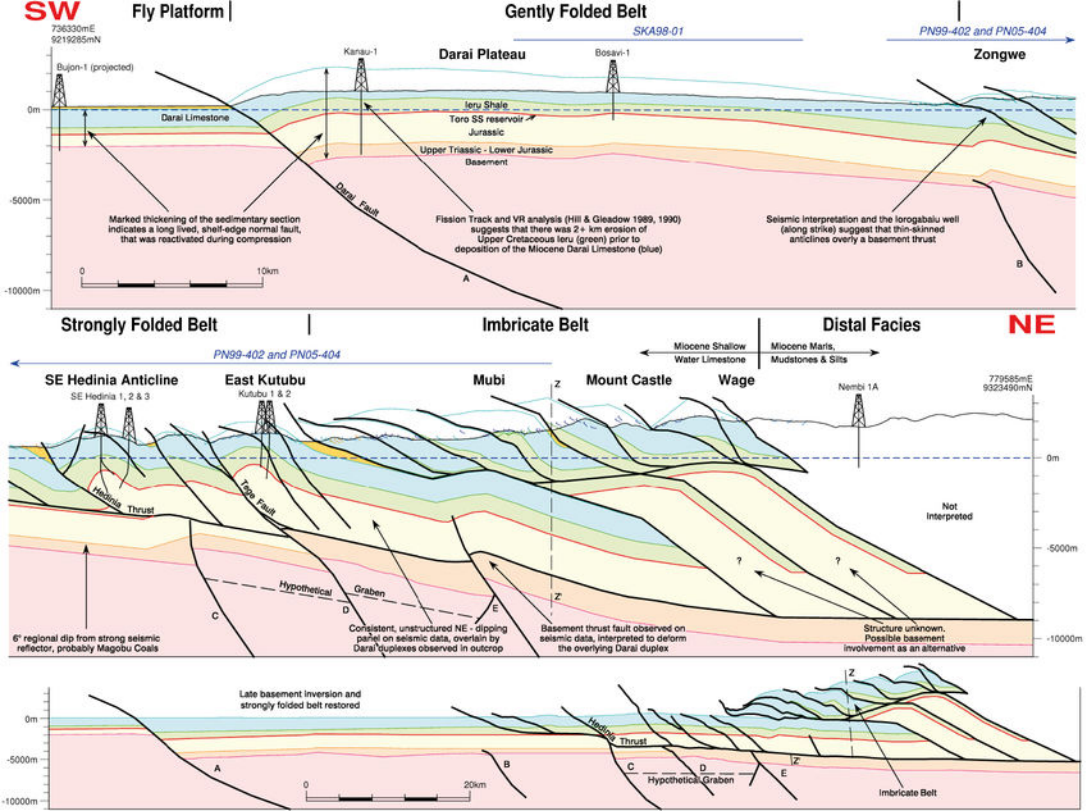
SW
736330mE
9219285mN
Fly Platform
Gently Folded Belt
SKA98-01
PN99-402 and PN05-404
Bujon-1 (projected)
Kanau-1
Darai Plateau
Bosavi-1
Zongwe
0m
-5000m
-10000m
Darai Limestone
Ieru Shale
Toro SS reservoir
Jurassic
Upper Triassic - Lower Jurassic
Basement
Darai Fault
Marked thickening of the sedimentary section indicates a long lived, shelf-edge normal fault, that was reactivated during compression
Fission Track and VR analysis (Hill & Gleadow 1989, 1990) suggests that there was 2+ km erosion of Upper Cretaceous Ieru (green) prior to deposition of the Miocene Darai Limestone (blue)
Seismic interpretation and the Iorogabalu well (along strike) suggest that thin-skinned anticlines overly a basement thrust
0
10km
A
B
Strongly Folded Belt
Imbricate Belt
Distal Facies
NE
PN99-402 and PN05-404
Miocene Shallow Water Limestone
Miocene Marls, Mudstones & Silts
SE Hedinia Anticline
SE Hedinia 1, 2 & 3
East Kutubu
Kutubu 1 & 2
Mubi
Mount Castle
Wage
Nembi 1A
779585mE
9323490mN
Hedinia Thrust
Toro Fault
Hypothetical Graben
Not Interpreted
6° regional dip from strong seismic reflector, probably Magobu Coals
Consistent, unstructured NE - dipping panel on seismic data, overlain by Darai duplexes observed in outcrop
Basement thrust fault observed on seismic data, interpreted to deform the overlying Darai duplex
Structure unknown. Possible basement involvement as an alternative
Late basement inversion and strongly folded belt restored
20km
Imbricate Belt

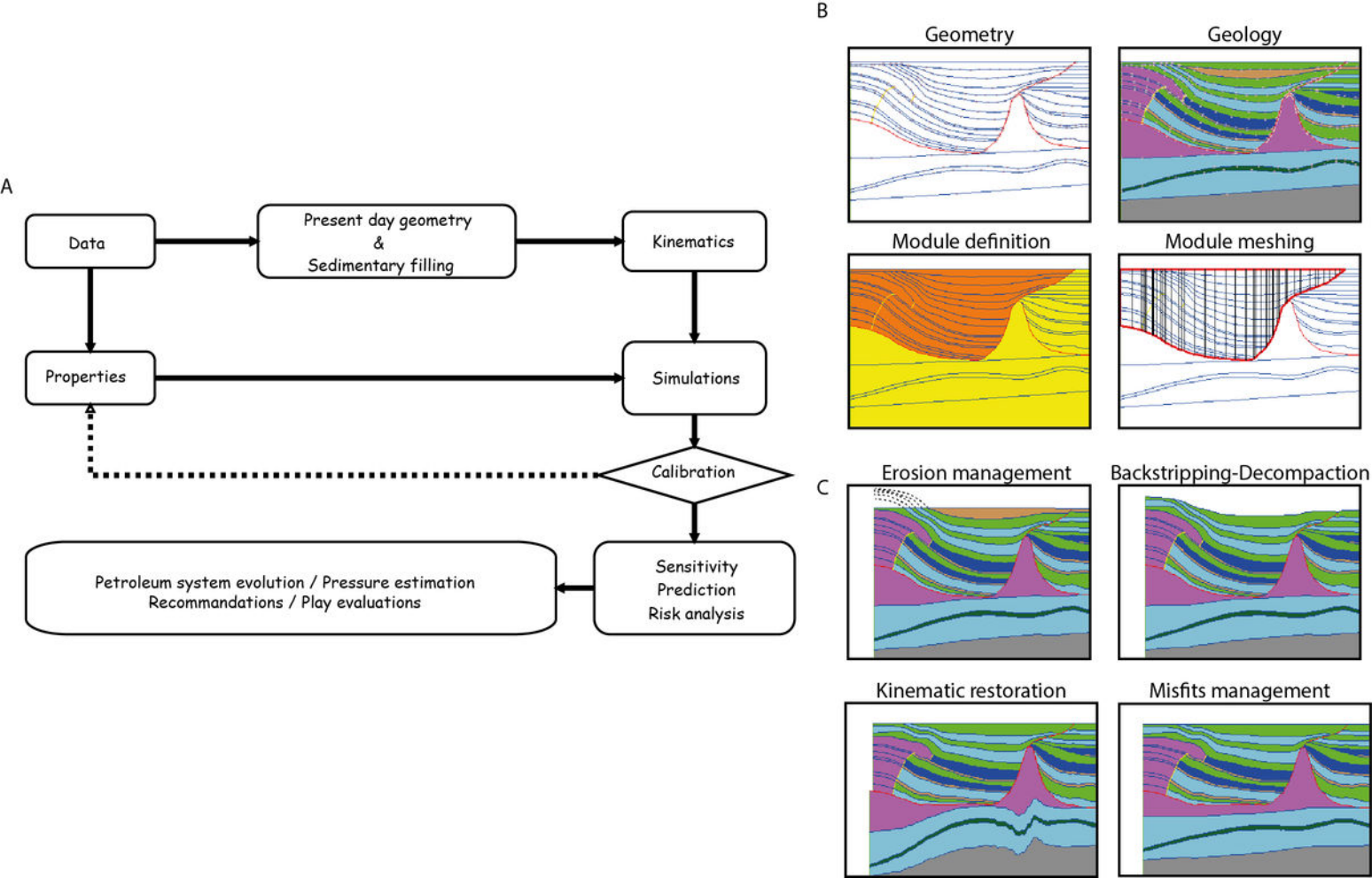
A
Data
Present day geometry
&
Sedimentary filling
Kinematics
Properties
Simulations
Calibration
Petroleum system evolution / Pressure estimation
Recommandations / Play evaluations
Sensitivity
Prediction
Risk analysis
B
Geometry
Geology
Module definition
Module meshing
C
Erosion management
Backstripping-Decompaction
Kinematic restoration
Misfits management

A

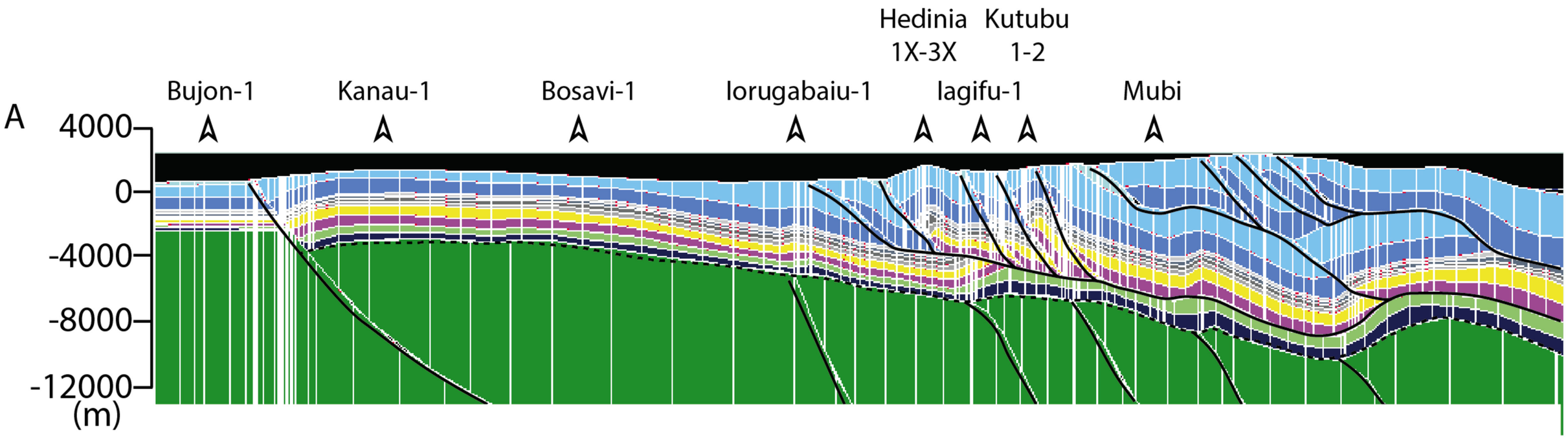

Orubadi
Darai
Ieru
Toro
Iagifu
Koilangi
Synrift
Upper crystaline crust
Fault
Decollement

B

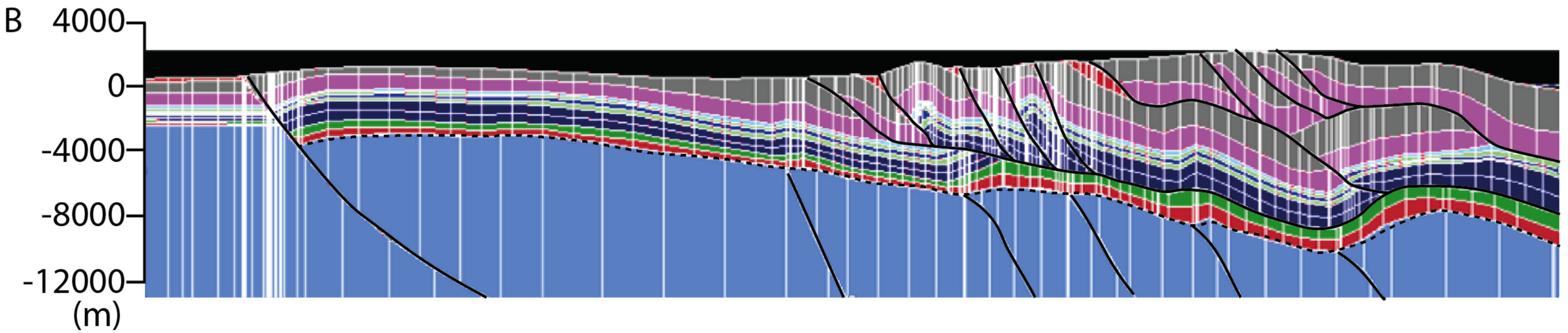

90%Sand - 10%Shale
70%Sand - 30%Shale
50%Sand - 50%Shale
30%Sand - 70%Shale
Shale
Limestone
Toro sandstone
Upper crystaline crust

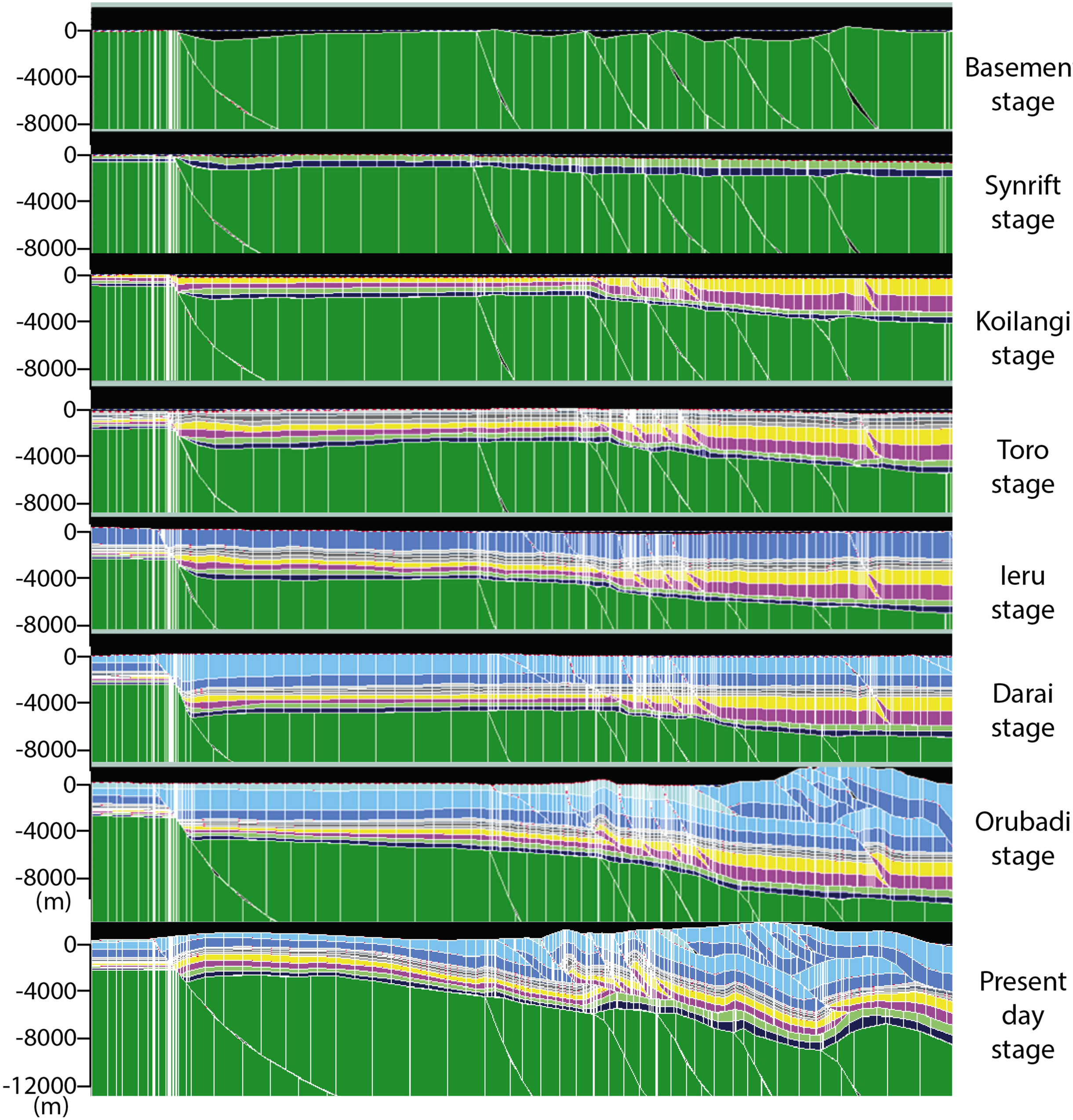
0
-4000
-8000
Basement stage
Synrift stage
Koilangi stage
Toro stage
Ieru stage
Darai stage
Orubadi stage
(m)
-12000
Present day stage
Orubadi
Darai
Ieru
Toro
lagifu
Koilangi
Synrift
Upper crystaline crust
Fault
Decollement

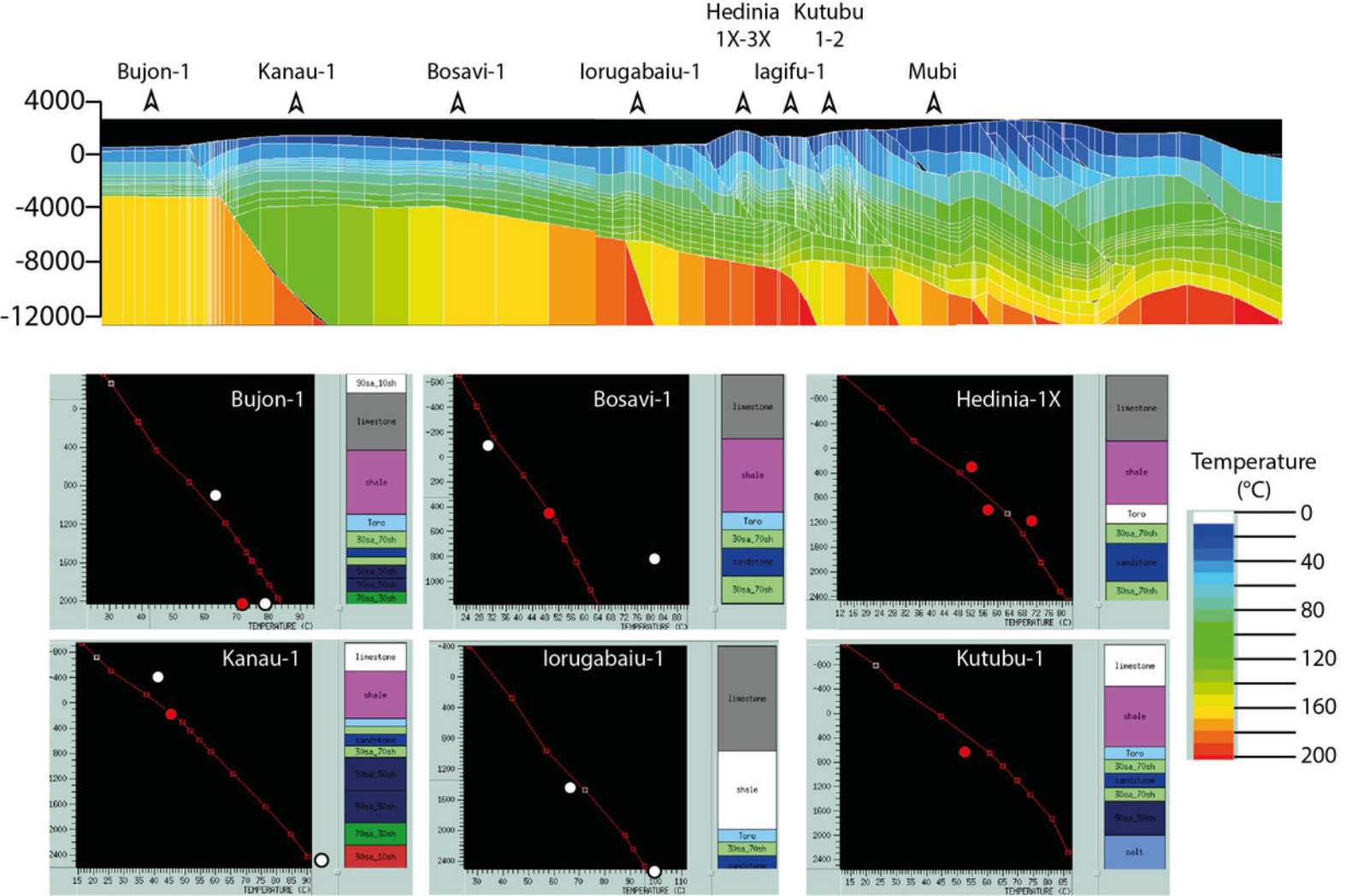
Bujon-1
Kanau-1
Bosavi-1
Iorugabaiu-1
Hedinia 1X-3X
Kutubu 1-2
Iagifu-1
Mubi
4000
0
-4000
-8000
-12000
Bujon-1
Bosavi-1
Hedinia-1X
Kanau-1
Iorugabaiu-1
Kutubu-1
TEMPERATURE (C)
limestone
shale
Toro
sandstone
salt
Temperature (°C)
0
40
80
120
160
200

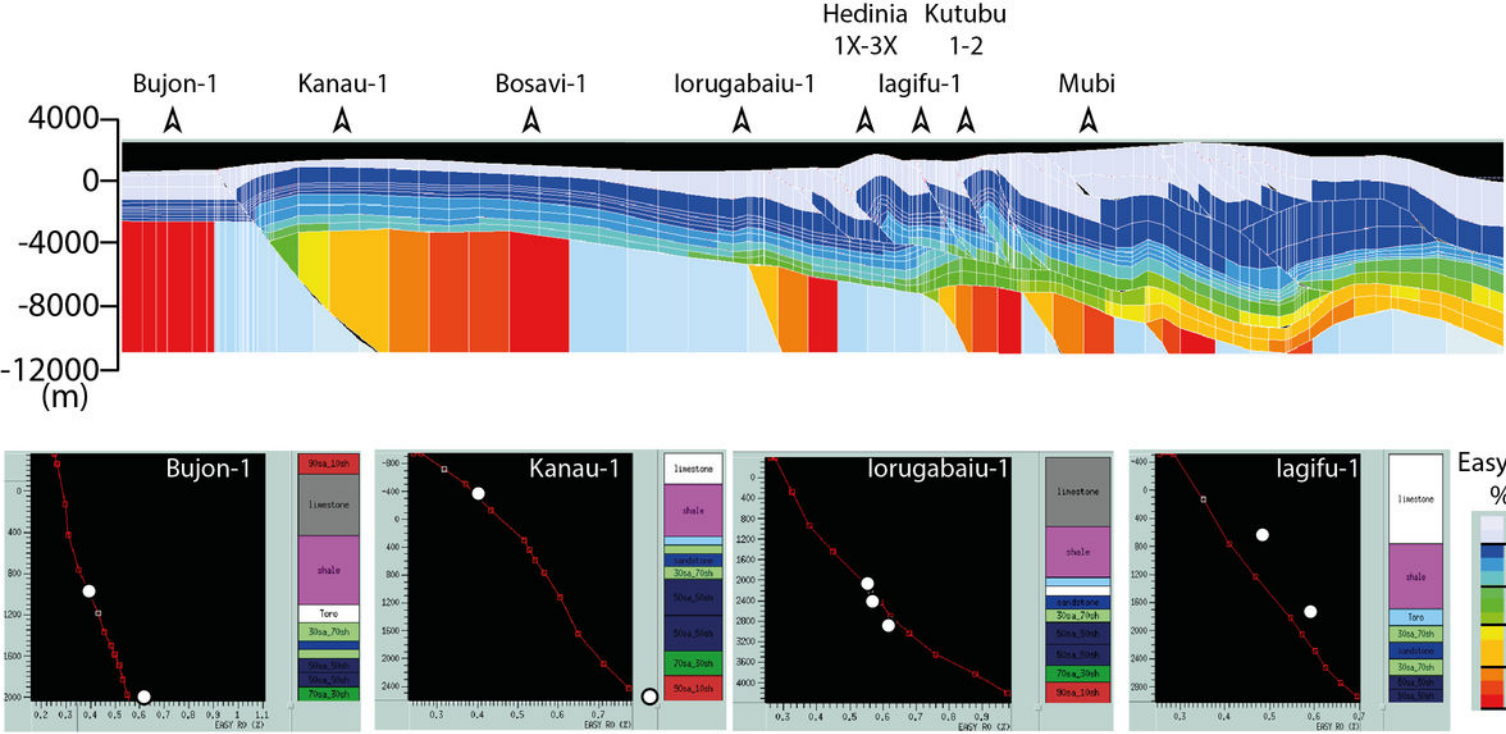
Hedinia
1X-3X
Kutubu
1-2
Bujon-1
Kanau-1
Bosavi-1
Iorugabaiu-1
Iagifu-1
Mubi
4000
0
-4000
-8000
-12000
(m)
Bujon-1
Kanau-1
Iorugabaiu-1
Iagifu-1
limestone
shale
Toro
sandstone
Easy Ro
%
0.4
0.8
1.1
1.4
2

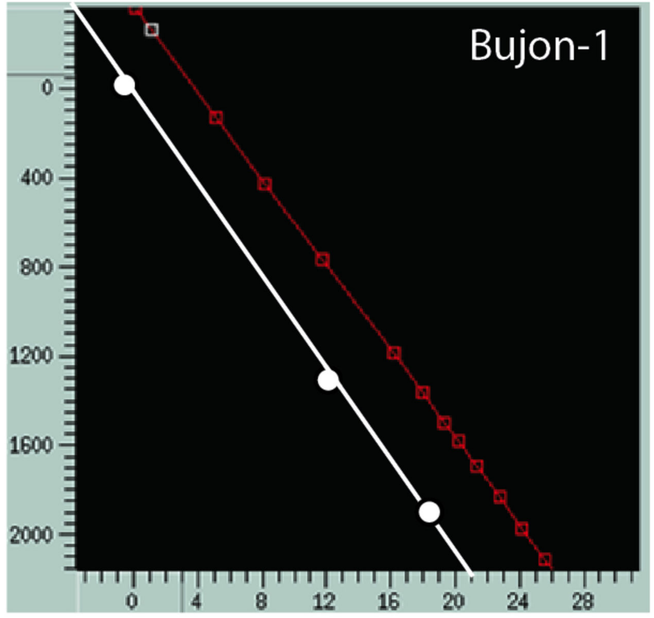

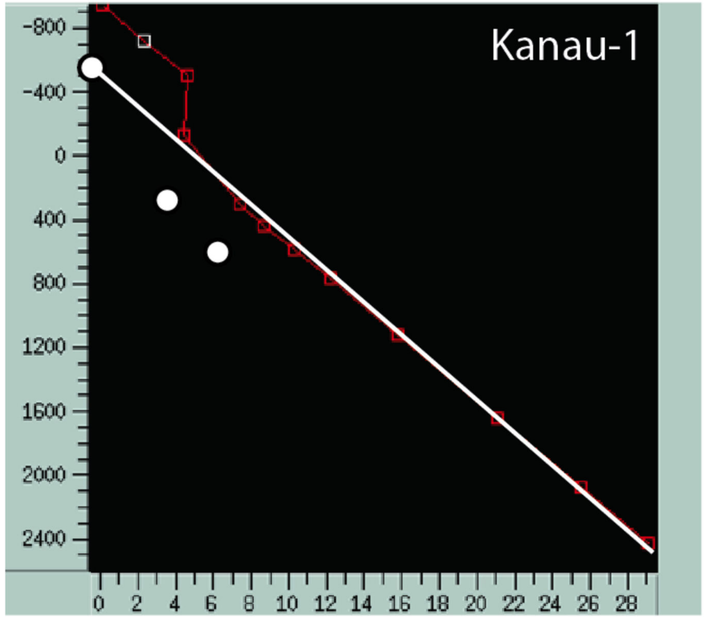

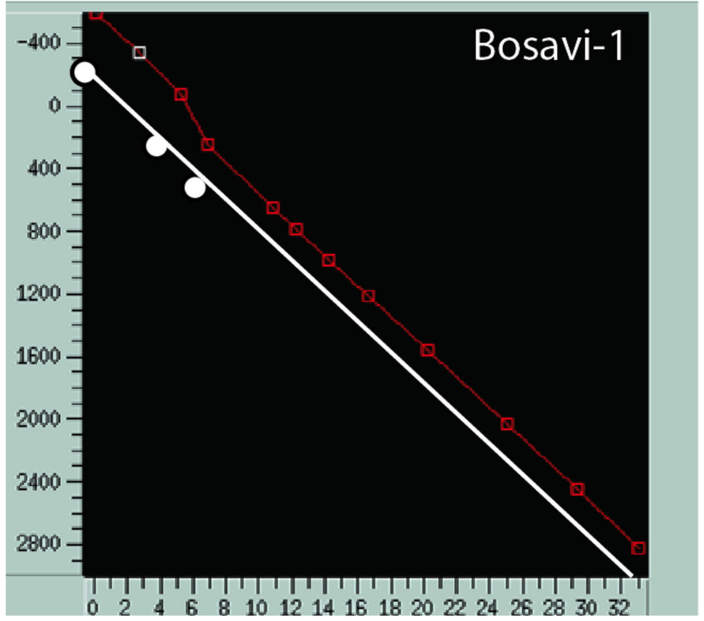

Hedinia Kutubu
1X-3X 1-2

Bujon-1 Kanau-1 Bosavi-1 Iorugabaiu-1 Iagifu-1 Mubi

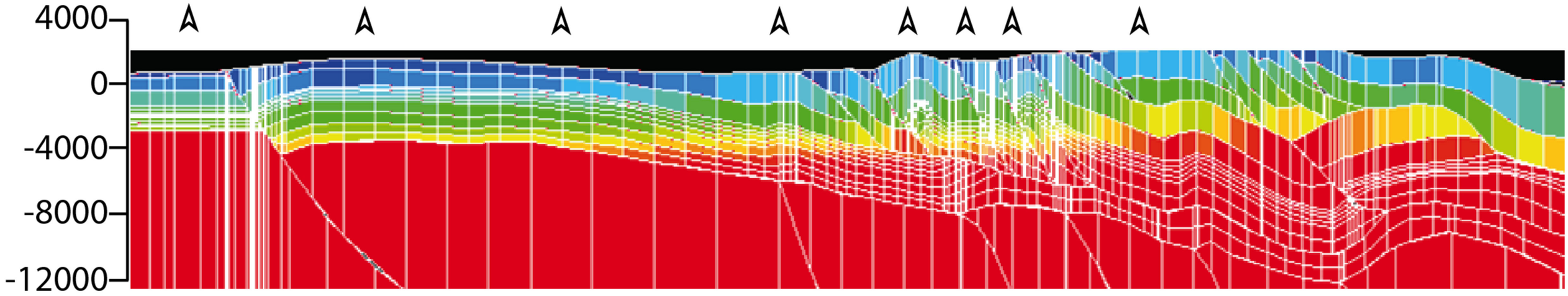

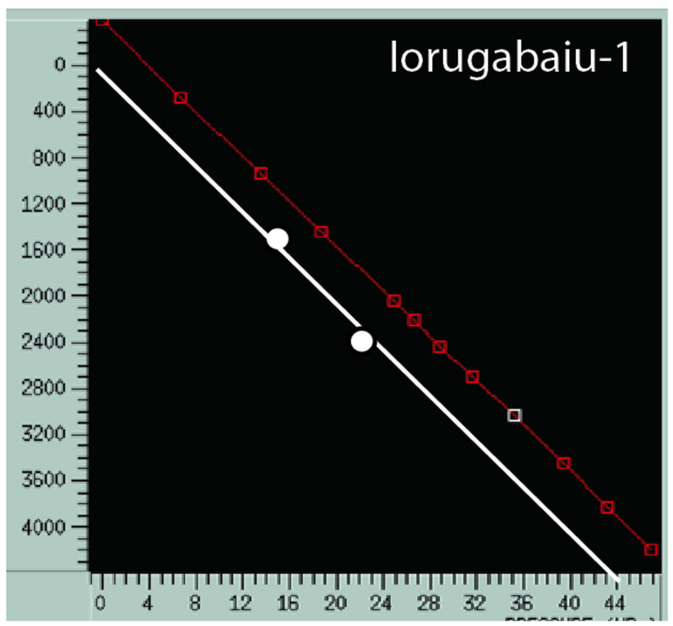

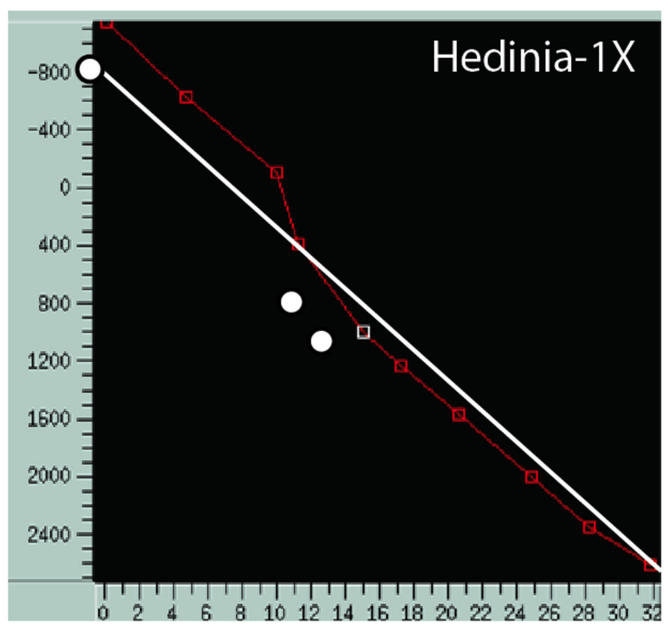

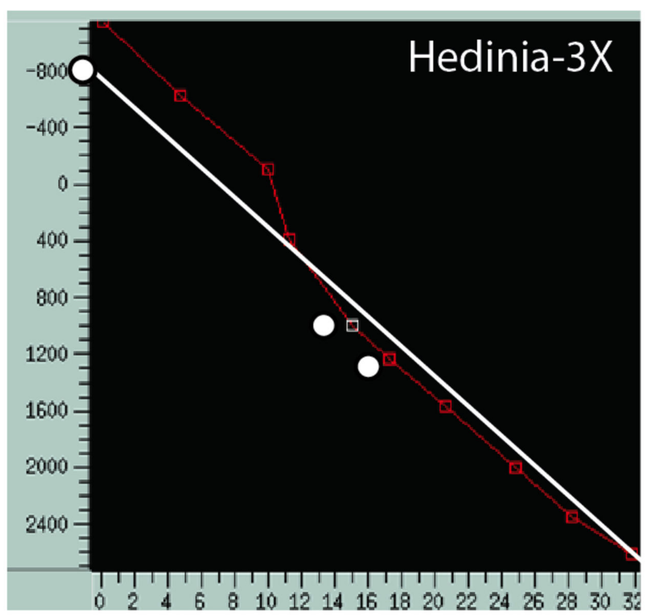

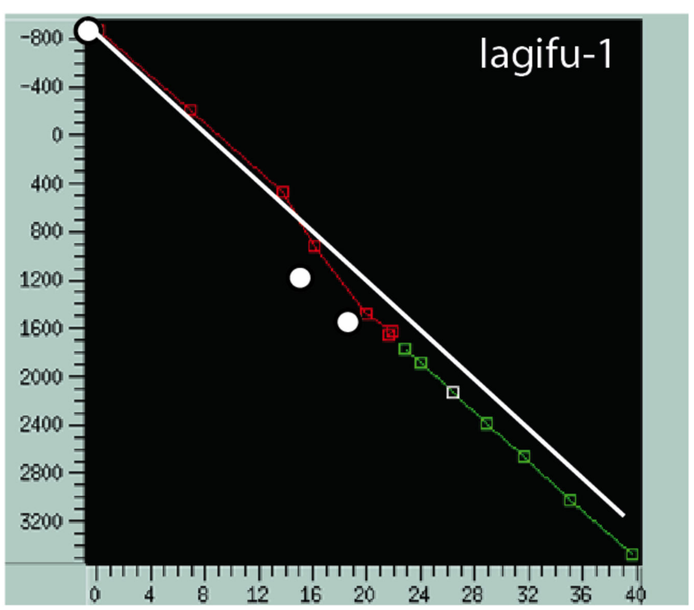

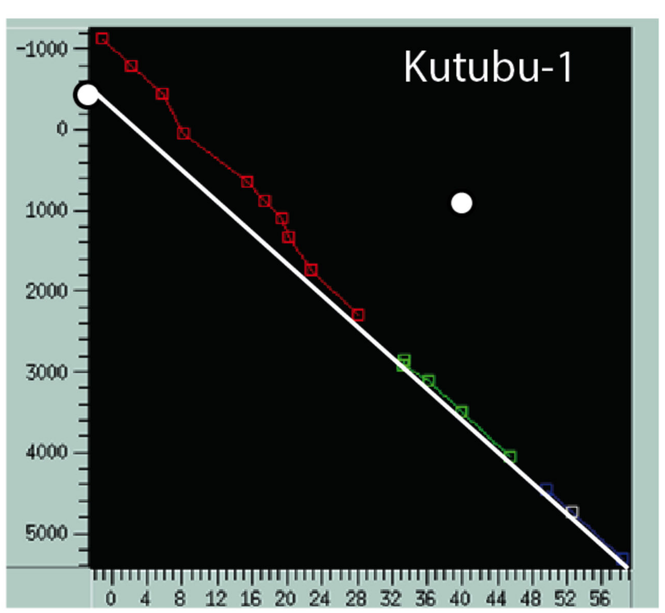

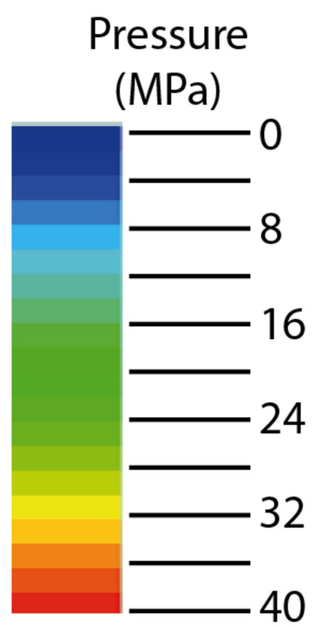

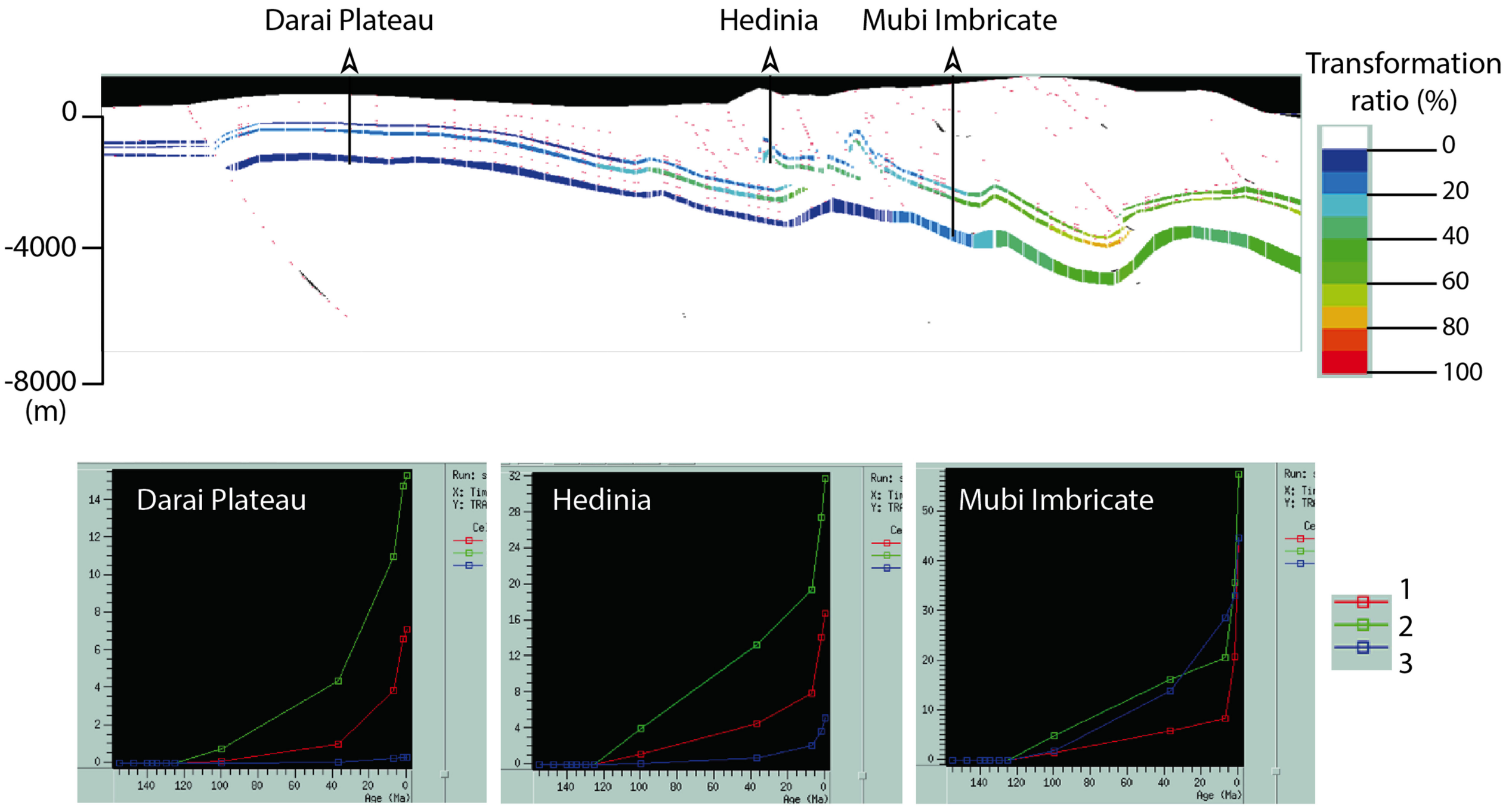
Darai Plateau
Hedinia
Mubi Imbricate
0
-4000
-8000
(m)
Transformation ratio (%)
0
20
40
60
80
100
Darai Plateau
Hedinia
Mubi Imbricate
Age (Ma)
1
2
3

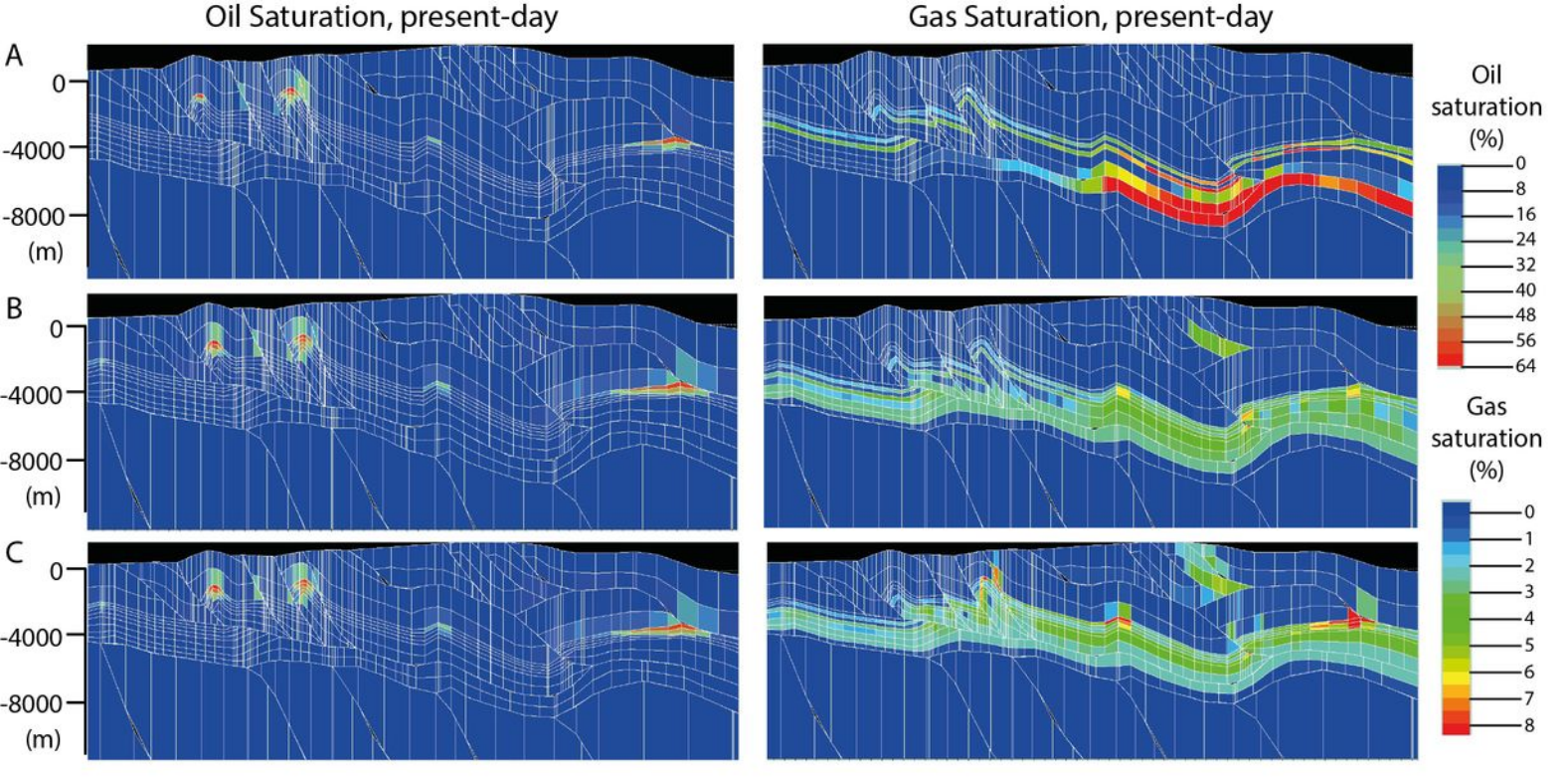
Oil Saturation, present-day
Gas Saturation, present-day
A
B
C
0
-4000
-8000
(m)
Oil saturation (%)
0
8
16
24
32
40
48
56
64
Gas saturation (%)
0
1
2
3
4
5
6
7
8

0
-4000
-8000
(m)
7
8
6
5
5
Present-Day
0
-4000
-8000
(m)
4
8
3
2
2
Orubadi stage
0
-4000
-8000
(m)
1
Darai Stage
Hydraulic head (MPa)
0
4
8
12
16
20